Department of Physics and Astronomy
University of Heidelberg

Bachelor Thesis in Physics
submitted by

Maja Isabelle Rüth

born in Mainz (Germany)

2021

Characterisation of a chemiluminescence ozone monitor for volcanic applications

This Bachelor Thesis has been carried out by Maja Isabelle Rüth at the
Institute for Environmental Physics (IUP) in Heidelberg
under the supervision of
Prof. Ulrich Platt

Abstract

Volcanic plumes are known to contain reactive halogen species, especially bromine monoxide, which are known to efficiently catalyse ozone (O_3) destruction. Therefore, local O_3 depletion is expected inside volcanic plumes, which has been measured in several field studies and is also found in several modelling studies. Recently, in order to quantify O_3 mixing ratios in volcanic plumes, mainly UV absorption monitors have been used as these have become the standard technique for ambient O_3 monitoring. However, these instruments show a large positive interference with sulfur dioxide (SO_2), which is difficult to correct. This poses a significant problem for volcanic measurements since SO_2 mixing ratios can exceed O_3 mixing ratios by factors of 1000 or more.

This interference problem can be solved by using the 'antiquated' technique of chemiluminescence (CL) O_3 monitors since these devices have been shown to exhibit no interference from trace gases contained in volcanic plumes - in particular SO_2. In this thesis, a compact and mobile (backpack-size, 10kg) CL monitor is introduced and characterised. The results of O_3 measurements in ambient air and inside the plume emanating from a fumarole at the summit of Mt. Etna volcano, Italy with the CL monitor are compared to those of a conventional UV absorption monitor. In this first field study inside a fumarole, no significant interference with volcanic SO_2 concentrations for the CL monitor was observed. Additionally, a rough calculation to estimate the expected O_3 depletion in volcanic plumes was made. Contrary to popular belief, this calculation suggests no significant reactive halogen catalysed O_3 loss (i.e. $\approx 1\%$) in volcanic plumes for typical bromine monoxide concentrations.

Zusammenfassung

Vulkanfahnen enthalten reaktive Halogenverbindungen, insbesondere Brommonoxid, welche den Abbau von Ozon (O_3) katalysieren. Deshalb ist ein lokaler Abbau von O_3 in Vulkanfahnen zu erwarten. Dieser wurde in mehreren Feldmessugen und auch in Modellstudien nachgewiesen. In den letzten Jahren wurden hauptsächlich Ultraviolett (UV) Absorption Ozon Monitore verwendet um O_3 in Vulkanfahnen zu messen. Diese Geräte werden standardmäßig in der Untersuchung der Umgebungsluft verwendet, zeigen aber eine signifikante Interferenz mit Schwefeldioxid (SO_2), welche nur schwer zu korrigieren ist. Das stellt ein Problem für Messungen in Vulkanfahnen dar, da dort SO_2 Mischungsverhältnisse diese von O_3 um den Faktor 1000 oder mehr übersteigen können.

In dieser Arbeit wird ein mobiler (Rucksackgroß, 10kg) Chemolumineszenz (CL) Ozon Monitor vorgestellt und charakterisiert. Die Wahl fiel auf ein CL Gerät, da gezeigt wurde, dass diese keine Interferenz mit Spurengasen aus Vulkanfahnen aufweisen. Die Ergebnisse der O_3 Messungen mit dem CL Monitor in Umgebungsluft und in einer Fumarole am Krater des Ätnas, Italien, werden mit denen eines UV-Absorption Monitors verglichen. Diese erste Feldmessung in der Fahne einer Fumarole zeigt tatsächlich keine Interferenz des CL Monitors mit vulkanischen Spurengasen.
Zusätzlich wird eine Überschlagsrechnung vorgestellt, die den O_3 Abbau in der Fahne abschätzt. Diese Rechnung zeigt, entgegen der allgemeinen Meinung, dass für typische Brommonoxid Konzentrationen kein signifikanter, durch reaktive Halogenverbindugen katalysierter O_3 Abbau ($\approx 1\%$) zu erwarten ist.

Contents

1 Introduction

Volcanic gas measurements are of interest for several reasons. Especially from a volcanological point of view volcanic gas emission measurements play an important role in understanding volcanoes and might even allow an insight into the volcanoes magmatic system itself (see e.g. Burton et al., 2007). Volcanic plume gas measurements can be an important tool for volcanic monitoring, for instance, the gas composition has often been observed to change prior to an eruption.

Another reason for measuring volcanic gas emissions is their impact on the atmosphere and their climatic relevance. Volcanoes emit large amounts of water vapour, carbon dioxide (CO_2), sulphur species, in particular sulfur dioxide (SO_2) and hydrogen sulfide (H_2S) and hydrogen halides. Also, they are potentially an important source of reactive halogen species in the troposphere and stratosphere. Reactive halogen species and especially bromine (bromine radical (Br), bromine monoxide (BrO)), play an important role in many reaction cycles in the atmosphere and account for significant parts of the reduction of stratospheric ozone (O_3), change the OH/HO_x ratio and can also interfere with the NO_x reaction cycle (Platt and Bobrowski, 2015).

Due to bromine catalysed O_3 destruction (see Sec. 2.3), local depletion of O_3 in the plume is expected. Several studies located at different volcanoes with varying approaches have been conducted to verify this predicted O_3 depletion within volcanic plumes. A comprehensive list of published articles on this subject is shown in Tab. 1. It is an extension to the existing table of reported O_3 depletion in Surl et al. (2015).

Great variation in the observed O_3 depletion is reported with studies showing no O_3 depletion (see e.g. Roberts, 2018) and other studies showing an O_3 depletion of up to 90% of ambient values (see e.g. Hobbs et al., 1982).
Some differences arising between studies might be explained with the fact that different volcanoes were studied. This is particular emphasised by the measurements of Roberts (2018). In this study measurements of O_3 at Kīlauea were conducted. As Kīlauea is thought to be a low halogen emitting volcano, the insignificant O_3 depletion is accounted for by low abundances of reactive halogen species.

Strong variability of the in-plume O_3 loss can not only be observed between studies at different volcanoes but also in studies conducted at the same volcano. For instance, when gas measurements are conducted in plumes of different age, or during different emission phases, the measurements of the in plume O_3 mixing ratios show significant differences (e.g. Hobbs et al., 1982; Fruchter et al., 1980).

Several sources state that they can not attribute the observed O_3 depletion solely to chemical reactions in the plume since ambient conditions also play an essential role and have to be considered when interpreting measurement data. In particular, ambient mixing ratios of O_3 and the mixing of ambient air into the volcanic plume influence the observed values of O_3 mixing ratios in the plume. Therefore, monitoring of ambient conditions is crucial in order to correctly interpret the data obtained from measurements of volcanic plumes. From this data then the effect of reactive halogen catalysed O_3 loss and the effect from anomalies of ambient O_3 mixed into the plume can be better estimated or simulated with corresponding numerical models. Kelly et al. (2013) have taken this approach of separating chemical loss and O_3 anomalies caused by mixing of volcanic gases and air. This study stresses the importance of ambient conditions on the observed O_3 depletion.

location	Measurement platform	instrument type	ozone depletion [%]	remark	reference
Etna	ground based	UV absorption (2B Technologies, model 202)	15-45	use of two CrO_3 scrubbers in series	Surl et al. (2015)
Augustine (1976)	airborne	CL (Monitor Labs model 841ßA, ethylene)	average: 60	large variability (0-100), plume aged several hours	Vance et al. (2010)
Etna (2004, 2009)	ground based	UV absorption (2B Technologies)	15-40	use of CrO_3 scrubber, depletion within in tens of seconds from crater	Vance et al. (2010)
Eyjafjallajökull (2010)	airborne	UV absorption (dual cell, Thermo Environmental Instruments Inc. Models 49C)	4-84 (per transect)	mean: 47 standard deviation: 21, depletion maintained in 1-9 days old plume, strong anti correlation with SO_2	Vance et al. (2010)
Kīlauea	ground based	electrochemical (Aeroqual instrument, WO_3 sensor)	no depletion	Kilauea is a low halogen emitter	Roberts (2018)
Sakurajima	ground based	UV absorption (Thermo Environmental instrument, model 49)		rapid decrease of O_3 for increase in SO_2	Lee et al. (2005)
Redoubt (2010)	airborne	UV absorption (2B Technologies, Inc., Model 205)	80	data post processing; entertainment of ambient air and chemical O_3 loss have to be separated; chemical loss: 1-16 ppb	Kelly et al. (2013)
St. Helens (200 km downwind)	airborne	?	33-70		Fruchter et al. (1980)
St. Helens (33 km downwind)	airborne	CL (Monitor Labs model 8410A, ethylene)	max. 90	depletion for phreatic emissions, no depletion for paroxysmal or intra-eruptive emissions	Hobbs et al. (1982)
Mt. Erebus (2005)	airborne	UV absorption	35	depletion only observed when SO_2 exceeds 20 ppb	Boichu et al. (2011)
Tungurahua (Ecuador)	airbrone	CL (FastOz, Nitric Oxide)	20-30	data insufficient to attribute all depletion to chemical reactions	Carn et al. (2011)

Table 1: Compilation of measurements reporting O_3 depletion. The approaches taken to measure the O_3 depletion as well as their actual values vary greatly. Table adapted from Surl et al. (2015).

All of the above mentioned factors (by no means exhaustive) show the complex processes influencing plume chemistry and with it O_3 mixing ratios. With this the need for reliable and most importantly more measurements of O_3 in volcanic plumes becomes apparent. Further measurements are needed to verify existing theories and crosscheck model calculations.
For instance, monitoring of volcanic O_3 might provide further insights into the formation of BrO from HBr as it is still an unanswered question to what extend its formation might be limited by O_3.

The majority of the referenced articles report the use of an ultraviolet (UV) absorption instrument to monitor the O_3 mixing ratios. These monitors, however, show significant positive interference to SO_2. Under normal atmospheric conditions this does not play a major role since O_3 mixing ratios ($\approx$40 ppb) exceed the mixing ratio of SO_2 ($<$1 ppb) and the sensitivity of the UV absorption monitor to SO_2 is reduced by roughly a factor of 100 compared to the sensitivity to O_3. However, when measuring volcanic emissions, SO_2 mixing ratios might reach values in the ppm regime and therefore exceed O_3 mixing ratios by factors of 1000 or more. Even with the reduced sensitivity for SO_2, this still leads to apparent O_3 mixing ratios of several tens or hundreds of ppb. Therefore, techniques to counteract this positive interference have to be employed (post processing: Kelly et al. (2013), selective SO_2 scrubber: Surl et al. (2015), Vance et al. (2010)), which introduce additional error sources (see Sec. 4.2.2).

A good way to overcome this problem without introducing further potential uncertainties is to use an O_3 monitor relying on chemiluminescence (CL). This method was the standard technique in the 1970s and 1980s and is now revisited for its advantages, those being no known inferences from trace gases abundant in volcanic plumes Rüdiger et al. (2020). CL O_3 monitors are therefore a promising alternative to the conventional UV absorption instruments for studies of O_3 in volcanic plumes. However, only few studies in volcanic plumes using CL monitors have been conducted (Hobbs et al., 1982; Vance et al., 2010; Carn et al., 2011) , probably since CL monitors are usually heavy and bulky and therefore make field measurements even more difficult as their use generally entails high infrastructural effort such as airborne measurements.

In this thesis a portable CL O_3 monitor is characterised (Sec. 5) and compared to a standard UV absorption monitor (Sec. 7). The applicability of both monitors for volcanic gas emission measurements is tested with measurements of O_3 inside a fumarolic plume (Sec. 8). Furthermore, a rough calculation is made to estimate the expected O_3 depletion in volcanic plumes for typical BrO mixing ratios (Sec. 3). From this calculation the somewhat surprising conclusion can be drawn that no significant O_3 depletion should be expected.

2 Theoretical background

2.1 Composition of the atmosphere

The composition of the atmosphere is important as it influences, for instance, the energy budget of the earth (greenhouse effect, anthropogenic climate change) and determines the air quality.
The main components of the atmosphere are nitrogen (N_2) (78.09 vol.-%), oxygen (O_2) (20.95 vol.-%) and argon (Ar) (0.93 vol.-%), followed by neon, helium, krypton and xenon. The mixing ratios of these inert components are relatively constant and they are therefore considered permanent constituents of the atmosphere.
Apart from these permanent constituents there are so called trace substances, including aerosols as well as trace gases. These trace substances account for a majority of the effects mentioned above, such as air quality and greenhouse effect. Concentrations of trace substances undergo temporal and spatial variations. The lifetime of some of these species can be relatively short with ranges in the order of hours (e.g. formaldehyde) or days (e.g. SO_2). Other trace gas species, however, are long-lived with lifetimes on the order of several years (e.g. CO_2 and methane). The main trace gases are water vapour, CO_2, methane and O_3 (Roedel and Wagner, 2017).

One parameter influencing the temporal and spatial variations as well as the lifetime of trace gases are chemical reactions in the atmosphere. Often, free radicals (neutral fragments of molecules containing an unpaired electron causing them to be very reactive) play a crucial role in these reactions, either as reactants, products or both. In particular, the reaction rates with which these reactions take place strongly influence the lifetime of trace gas species and free radicals. The rate of a reaction is the rate of the decrease or increase of the reactants concentration over time (Donaldson and Wren, 2015).
This is where reaction kinetics come into play.

2.2 Reaction kinetics

The field of chemical or reaction kinetics is dedicated to investigate 'the rates of transformation of chemical compounds from reactant species into products' (Donaldson and Wren, 2015). Consider an arbitrary chemical reaction,

$$\mathrm{aA} + \mathrm{bB} \longrightarrow \mathrm{cC} + \mathrm{dD} \tag{1}$$

where small letters denote the stoichiometric coefficients (number of molecules of the respective compound) and capital letters the respective compounds. The reaction velocity, also called the reaction rate, is then given by the following expression (Bechmann and Bald (2017), Donaldson and Wren (2015)) :

$$\mathrm{Rate} = v_R = -\frac{1}{\mathrm{a}} \cdot \frac{d[\mathrm{A}]}{dt} = -\frac{1}{\mathrm{b}} \cdot \frac{d[\mathrm{B}]}{dt} = \frac{1}{\mathrm{c}} \cdot \frac{d[\mathrm{C}]}{dt} = \frac{1}{\mathrm{d}} \cdot \frac{d[\mathrm{D}]}{dt} \tag{2}$$

Here, $[A]$-$[D]$ are the concentrations of the compounds given in $[\mathrm{molec} \cdot \mathrm{cm}^{-3}]$, v_R is given in units of $[\mathrm{molec} \cdot \mathrm{cm}^{-3} \cdot \mathrm{s}^{-1}]$.

The rate can also be expressed in dependence of the reactants concentration and not only as a function of their temporal derivation. This can be intuitively established when understanding that chemical reactions usually involve collisions or close approaches of the reagents in order to proceed. In the gas phase the probability for collisions is proportional to the concentration of the compounds and therefore the reaction rate can be expressed by means of it as well

$$\text{Rate} = k \cdot [\text{A}]^a[\text{B}]^b \qquad \text{and} \qquad a + b = n. \tag{3}$$

The proportionality factor k, the so called rate constant, is given in $[\text{molec}^{1-\text{n}} \cdot \text{cm}^{3\text{n}-3} \cdot \text{s}^{-1}]$. The reaction order n can be determined by summing over the exponents a and b.

Here, we will only consider elementary reactions for which the time dependent concentrations is obtained by integrating the differential equation which is given by Eqn. 3 together with Eqn. 2. This differential equation is called the rate expression and is given by

$$-\frac{1}{\text{a}} \cdot \frac{d[\text{A}]}{dt} = k \cdot [\text{A}]^a[\text{B}]^b. \tag{4}$$

Elementary reactions can be divided into three types: first-order, second-order and third-order reactions. All tree types are listed in Tab. 2 with their corresponding rate and rate constants. The molecularity describes the number of reactants involved in the reaction and is given by the sum over the stoichiometric coefficients of the reactants. For elementary reactions the reaction order equals the molecularity (Bechmann and Bald, 2017).

To obtain the temporal evolution of the concentrations of the reactions listed in Tab. 2 the respective rate expressions (see Eqn. 4) have to be integrated. In an exemplary way, lets consider first order reactions for which the rate expression can be expressed as

$$-\frac{d[\text{A}]}{dt} = k_1 \cdot [\text{A}]. \tag{5}$$

This differential equation can be solved by separation of variables which then yields the time dependent concentration,

$$\ln\left(\frac{[\text{A}]}{[\text{A}]_0}\right) = -k_1 \cdot t \quad \rightarrow \quad [\text{A}](t) = [\text{A}]_0 \cdot \exp\left(-k_1 \cdot t\right), \tag{6}$$

where $[\text{A}]_0$ denotes the starting concentration.

order	types	scheme	rate	reaction constant
first order	unimolecular photochemical transformation	$\text{A} \longrightarrow \text{B}$ $\text{A} + \text{h}\nu \longrightarrow \text{B}$	$k_1 \cdot [\text{A}]$	s^{-1}
second order	bimolecular (different reagents and self reactions)	$\text{A} + \text{B} \longrightarrow \text{C}$	$k_2 \cdot [\text{A}] \cdot [\text{B}]$	$\text{cm}^3\text{molec}^{-1}\text{s}^{-1}$
third order	trimolecular	$\text{A} + \text{B} + \text{C} \longrightarrow \text{D}$	$k_3 \cdot [\text{A}] \cdot [\text{B}] \cdot [\text{C}]$	$\text{cm}^6\text{molec}^{-2}\text{s}^{-1}$

Table 2: List of elementary reactions with reaction schemes and the corresponding rates.

Apart from the dependence of the rate on the concentration there is also a temperature T dependence which has to be considered. This dependence is introduced through the rate constant k which directly depends on T. Most reactions exhibit an increase in rate for a rise in temperature ($\frac{dk}{dT} > 0$) (Bechmann and Bald, 2017). Svante Arrhenius established an empirical relation for k and T in 1889 known as the Arrhenius equation (exponential form) (Bechmann and Bald, 2017; Donaldson and Wren, 2015):

$$k(T) = k_0 \cdot exp\left(-\frac{E_A}{R \cdot T}\right) \tag{7}$$

where E_A is the activation energy, R is the gas constant and T the temperature in Kelvin.

Usually, the goal of kinetic studies is the clarification of complex reaction mechanisms. These usually include a series of consecutive reactions as elementary steps, yielding the total net reaction. A particularly helpful concept is the rate-determining step. It applies if the net reaction consists of a cascade of elementary reactions and one of these is significantly slower than the other reactions. It is plausible that this step then limits the net reaction (Bechmann and Bald, 2017). Hence, the net reaction rate can be approximated by the rate expression of the slowest proceeding reaction.

2.3 Volcanic plume chemistry

Quiescent degassing and erupting volcanoes often emit a multitude of trace gases and particles directly into the atmosphere. The mixture of volcanic gases with the surrounding atmosphere forms a very unusual composition which leads to very particular, still not fully understood chemical reactions. For instance, solid and liquid particles are available in vast abundances, which provide a large surface area for heterogeneous chemical reactions (reactions of gas molecules with reactant in liquid phase (Roedel and Wagner, 2017)) to take place. Also, high amounts of acids in form of HCl and H_2SO_4 are emitted or rapidly formed inside the plume. This accounts for the high acidity measured in close proximity to volcanoes (Bobrowski et al., 2007). Other compounds, such as SO_2 or highly reactive halogen species can be emitted in significantly higher abundances than usually found in the troposphere. These reactive halogen species (e.g. BrO) are of special interest as they are able to influence and catalyse several reaction cycles as well as change the oxidative capacity of the atmosphere (von Glasow, 2010; Kern et al., 2009). Therefore, quiescently degassing volcanoes are now known to have a significant impact on the troposphere.
Even larger chemical perturbations, but not as continuous as the effects of passively degassing volcanos, can be attributed to large explosive eruptions, which can not only effect the troposphere but also the stratosphere. For instance, if large amounts of ash and sulphur compounds (mainly SO_2) are injected into the stratosphere, they can influence the global aerosol layer at about 20 km altitude, called the Junge layer (von Glasow et al., 2009; Jourdain et al., 2016). These sulphur compounds are there converted into aerosols with residence times of 1-2 years and influence climate directly (through perturbations of Earth energy balance) and indirectly (coupling between radiation, microphysics and atmospheric chemistry) (Jourdain et al., 2016). This can cause significant climatic changes like surface temperature anomalies (Robock, 2000; von Glasow et al., 2009).

But also from a volcanological point of view volcanic plume chemistry is of relevance. With measurements of volcanic gas emissions insights into the volcano's magmatic system and processes can be gained. For example, Burton et al. (2007) have been able to infer information on the depth where strombolian activity is formed through measurements of the magmatic gas phase.

In the 1970s airborne studies of volcanic plumes were conducted (Radke et al., 1976; Hobbs et al., 1982). However, it was not until 20 years later that the strong impact on tropospheric chemistry has been discovered with the first measurement of BrO in a volcanic plume by Bobrowski et al. (2003). Ever since this discovery, BrO has been detected in numerous field study at a variety of volcanos worldwide (e.g. Kern et al., 2009).

Primary volcanic emissions comprise mainly the following species (in descending order): water vapour, CO_2, SO_2, H_2S, HCl, HF, H_2, CO and HBr (more species are emitted in lower abundances) (von Glasow et al., 2009; Rüdiger et al., 2020).
The hydrogen halides HCl and HBr are thought to be the main species of halogens emitted by volcanoes (Gerlach, 2004; Bobrowski et al., 2007; von Glasow, 2010). Reactive halogen species, such as BrO, are assumed not to be a primary product and therefore not abundant in the initial plume composition. They are rather the product of chemical processes of magmatic gases with atmospheric components occurring when ambient air is mixed into the plume (Bobrowski et al., 2007; Kern et al., 2009; Jourdain et al., 2016). In particular, through high temperature oxidative dissociation, which occurs as soon as volcanic gases are mixed with air, atomic halogen species (Cl, Br) can be produced (Bobrowski et al., 2007; Jourdain et al., 2016). They then react with O_3, available from further entrainment of ambient air into the plume (Reaction 12). BrO can react with HO_2 to form HOBr (Reaction 15), which can then in turn form Br_2 trough a heterogeneous reaction with Br^- and H^+ within volcanic sulfate aerosols. Br^- and H^+ are available from dissolved volcanic HBr. Br_2 is rapidly photolized to produce two Br atoms, which can then again react with O_3 to form BrO. This is the start of an autocatalytic reaction causing an exponential growth of BrO giving rise to the name 'bromine explosion'. This autocatalytic reaction mechanism, which is thought to be the reason for elevated BrO levels and O_3 depletion, was first observed during spring in the polar boundary layer (Barrie and Platt, 1997; Wennberg, 1999). In the following the reaction mechanism is shown (Bobrowski et al., 2007; von Glasow et al., 2009; von Glasow, 2010; Kern et al., 2009, and references therein),

$$\mathrm{HOBr(gas)} \longrightarrow \mathrm{HOBr(aq)} \tag{8}$$

$$\mathrm{HBr(gas)} \longrightarrow \mathrm{Br^-(aq) + H^+(aq)} \tag{9}$$

$$\mathrm{HOBr(gas) + Br^-(aq) + H^+(aq)} \longrightarrow \mathrm{Br_2(gas) + H_2O(gas)} \tag{10}$$

$$\mathrm{Br_2} + h\nu \longrightarrow \mathrm{2\,Br} \tag{11}$$

$$\mathrm{Br + O_3} \longrightarrow \mathrm{BrO + O_2} \tag{12}$$

$$\mathrm{BrO + BrO} \longrightarrow \mathrm{2\,Br + O_2} \tag{13}$$

$$\mathrm{BrO + BrO} \longrightarrow \mathrm{Br_2 + O_2} \tag{14}$$

$$\mathrm{BrO + HO_2} \longrightarrow \mathrm{HOBr + O_2} \tag{15}$$

$$\mathrm{BrO} + h\nu \longrightarrow \mathrm{Br + O} \tag{16}$$

reaction	k_{298} $[\mathrm{cm^3 \cdot molec^{-1}s^{-1}}]$	lifetime (for pseudo first order reaction)	lifetime [s] (1 ppb O_3)	lifetime [s] (40 ppb O_3)
$Br + O_3 \longrightarrow BrO + O_2$	k_1=1.2×10^{-12}	$t_{Br} = \frac{1}{k_1 \cdot [O_3]}$	35	0.9
$BrO + BrO \longrightarrow 2\,Br + O_2$	k_2=2.7×10^{-12}	$t_{BrO} = \frac{1}{k_2 \cdot [BrO]}$	38	38
$BrO + BrO \longrightarrow Br_2 + O_2$	k_3=4.8×10^{-13}	$t_{BrO} = \frac{1}{k_3 \cdot [BrO]}$	214	214

Table 3: Rate constants, reaction rates and corresponding time constants of the key reactions of the O_3 destruction mechanism. The lifetimes of Br and BrO for two O_3 mixing ratios, 1 ppb (low mixing ratio) and 40 ppb (usual ambient mixing ratio), and typically measured BrO concentration of 400 ppt ($9.7 \times 10^9\,\mathrm{cm^{-3}}$) are calculated. From the time constants, the BrO self reaction can be identified as the rate limiting step (even for very low O_3).

A key step in the 'bromine explosion' is the release of Br from HBr via reactions 9, 10, 11. For reaction 10 to proceed, particulate acidity, which is usually available in abundance, and HO_2 are needed. Further, mixing of air into the plume is crucial. Also, incident solar radiation is required so that Br_2 can be photolized to give Br. This is consistent with the finding of Kern et al. (2009) that BrO could not be detected during night time.

O_3 is assumed to be quickly destroyed in the plume due to reaction 12. The key steps in the destruction of O_3 are the reactions 12, 13, 14 (see e.g. von Glasow, 2010). In Tab. 3 the rate constants of these three reactions (Atkinson et al., 2000) are shown and the lifetimes of Br and BrO for the respective reactions are calculated. An extremely low O_3 mixing ratio (1 ppb, $[O_3] \approx 2.4 \times 10^{10}\,\mathrm{cm^{-3}}$) and atmospheric background amounts (40 ppb, $[O_3] \approx 9.7 \times 10^{11}\,\mathrm{cm^{-3}}$) as well as typically measured volcanic plume BrO mixing ratios (400 ppt, $[BrO] \approx 9.7 \times 10^9\,\mathrm{cm^{-3}}$) are assumed. The results show that for O_3 mixing ratios larger than 1 ppb the lifetime of Br is shorter than the lifetime of BrO. Therefore, the case of the rate-determining step described in Sec. 2.2 can be applied and the destruction of O_3 can be approximately quantified by the BrO self reaction and thereby by the measured BrO concentrations.

Thus, the process of O_3 depletion is limited by the recycling of Br atoms via the BrO self reaction. In model studies von Glasow (2010) found the self reactions of BrO to be responsible for about 84% of O_3 destruction in the first hour and 90% in the first six hours.
However, as we will present in the next section, rough calculations to estimate the influx of O_3 into the plume and its destruction inside it, approximated by the self reactions of BrO, suggest that for typical BrO concentrations no significant O_3 loss should be expected.

3 Plume mixing and estimated O_3 depletion

In order to fully understand the development of the volcanic plume not only the above explained plume chemistry is of importance but also physical processes such as the entrainment of ambient air into the plume. These physical processes significantly influence the occurring chemical processes in the plume as they determine the concentration of ambient air gas species available for chemical reactions. Their impact has been briefly touched upon in the previous section. This influence also becomes apparent with the fact that the chemical conditions transition rapidly from reducing to oxidising as soon as volcanic volatiles meet air (von Glasow, 2010).

The mixing processes in volcanic plumes are dominated by turbulent diffusion. Transport processes dominated by turbulent diffusion are significantly faster than those dominated by molecular diffusion, the latter is therefore only of minor importance in the troposphere. Randomly distributed fluctuations, a key characteristic of turbulence, complicate the description of the turbulent diffusion compared to the molecular diffusion. However, when considering stationary processes (time independent), a formula relying on the concentration gradient, analogous to Fick's first laws for the molecular diffusion, can be derived for the turbulent diffusion. This formula simplifies the handling of the otherwise rather complex and abstract formulas describing turbulent diffusion. The total diffusion can therefore be seen as the sum of turbulent and molecular diffusion and is given by Roedel and Wagner (2017):

$$j_{i,turbulent} = K_t \cdot \frac{dc_i}{dx} \quad \rightarrow \quad j_i = K \cdot \frac{dc_i}{dx} \tag{17}$$

with $K = D + K_t$, K_t the turbulent and D the molecular diffusion constant, j_i the flux of the considered species i and c_i its concentration.

In the following, a rough calculation to estimate the flow of O_3 into the plume and its depletion in the plume is sketched. It does not aspire to depict the complex processes in the plume in their entirety but rather identifies the dominating effects and estimates their impact on the plume composition.

We assume the plume geometry as given in Fig. 1 *left*. In Fig. 1 *right* the values of the parameters for two numerical examples, example 1 describes a young plume and example 2 an older plume, are given. Here, the plume is divided into two separate parts: the outer plume with a thickness of Δr and the inner plume, indicated by the solid line. Within the inner plume we assume no O_3 (consistent with the idea of local O_3 depletion in the plume). In ambient air a mixing ratio of 40 ppb is assumed (here, ppb is equivalently used for ppbv and denotes volume mixing ratios). This results in a concentration gradient driving the flux, which is assumed to only exist in the outer part of the plume and to be linear within it. In the inner plume as well as in the ambient air no concentration gradient is assumed.

With Fick's first law (Eqn.17), the lateral diffusion flux of ambient air and, in particular, of O_3 into the plume can be estimated when assuming stationary processes.
In the first step, the concentration gradient of O_3 has to be estimated.

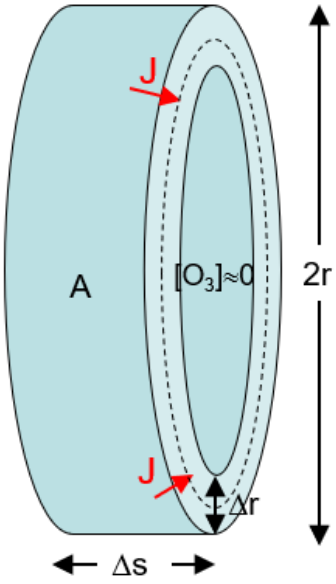

parameter	example 1	example 2
turbulent diffusion constant K_t	$10\,m^2\,s^{-1}$	$10\,m^2\,s^{-1}$
wind velocity v_p	$10\,m\,s^{-1}$	$10\,m\,s^{-1}$
plume age	125 s	12500 s
distance from crater	1.25 km	125 km
plume radius r	50 m	500 m
thickness outer plume Δr	20 m	200 m
time step Δt	1 s	1 s
plume width Δs	10 m	10 m
ambient $[O_3]$	40 ppb	40 ppb
in-plume $[O_3]$	0 ppb	0 ppb
in-plume [BrO]	400 ppt	400 ppt
O_3 flow into plume F	$1.25 \times 10^{21}\,s^{-1}$	$1.25 \times 10^{21}\,s^{-1}$
total O_3 destruction R	$1.6 \times 10^{19}\,s^{-1}$	$1.6 \times 10^{21}\,s^{-1}$

Figure 1: Assumed plume geometry and parameters.
left: Schematic of the plume geometry. The plume is divided into an outer plume section and an inner part, indicated by the solid line. Source: U.Platt, personal communication.
right: List of values of the parameters as used in the calculation. Additionally, the flow F of O_3 molecules into the plume and the destruction R in the inner plume are shown.

With the ideal gas law

$$pV = \nu RT = \frac{N}{N_A} RT, \tag{18}$$

where p is the pressure, V the volume and T the temperature of the gas, ν is the amount of substance in mole, N the number of molecules, N_A the Avogadro constant and R the gas constant, the concentration of O_3 can be calculated from its mixing ratio. Mixing ratios x are dimensionless and are calculated, in the case of volume mixing ratios, by $x_V = \frac{V}{V_{tot}}$.

$$[O_3] = \frac{N_{O_3}}{V_{air}} = \frac{\nu_{O_3} \cdot N_A}{V_{air}} = \frac{V_{O_3}}{V_{air}} \cdot \frac{p \cdot N_A}{RT} = x_V \cdot \frac{p \cdot N_A}{RT} \approx 1 \times 10^{12}\,cm^{-3} \tag{19}$$

Where $T \approx 300\,K$, $p \approx 1013\,hPa$, $R = 8.3145\,J\,mol^{-1}\,K^{-1}$ and an ambient O_3 mixing ratio of $x_V \approx 40\,ppb$ are assumed.

In the following, the values from example 1 are used, which correspond to a plume age of roughly $125\,s \approx 2\,min$. From the geometry of the plume and the concentration difference, the O_3 flux j into the inner plume can be calculated via Eqn. 17,

$$j = K_t \cdot \frac{\Delta c}{\Delta r} \approx 5 \times 10^{13}\,cm^{-2}\,s^{-1}. \tag{20}$$

Here, only the turbulent diffusion constant K_t is considered since the molecular diffusion constant D is reduced by 5 orders of magnitude compared to K_t within the troposphere and can therefore be neglected.

In a further approximation the area through which the flux of O_3 into the plume occurs is calculated. It can be assumed to lie in the middle of the outer plume and is indicated by the dotted line (see Fig. 1 *left*). Its width Δs is dependent on the wind velocity and the considered time step and can be calculated via $\Delta s = v_p \cdot \Delta t$. The area can then be calculated as follows

$$A = 2\pi \cdot (r - \frac{\Delta r}{2}) \cdot \Delta s \approx 2.5 \times 10^7 \,\mathrm{cm}^2, \tag{21}$$

allowing to estimate the flow F of O_3 molecules into the inner plume,

$$F = j \cdot A \approx 1.25 \times 10^{21} \,\mathrm{s}^{-1}. \tag{22}$$

Another way to evaluate the flow of O_3 molecules into the plume is by considering the evolution and expansion of the plume. To calculate the radius r of the plume the following formula can be applied

$$r^2 = 2 \cdot K \cdot t \tag{23}$$

with $K = D + K_t$.

This formula directly follows from the analogous treatment of turbulent and molecular diffusion. It was first derived by Einstein (1905).
Again, we will use the approximation $K \approx K_t$. For one time step Δt, the difference in radii of the plume can be calculated. This allows the calculation of the increase in the plumes cross section A and with that the volume ΔV mixed into the plume during the respective time step,

$$A(t) = \pi \cdot r^2 = 2\pi \cdot K \cdot t, \tag{24}$$

$$\Delta V = V(t + \Delta t) - V(t) = [A(t + \Delta t) - A(t)] \cdot v_p \cdot \Delta t = 2\pi \cdot K \cdot v_p \cdot \Delta t^2. \tag{25}$$

The volume with which the plume is diluted is independent of the specific time t and only depends on the time step Δt and the wind velocity v_p.
For the assumed values for the young plume (example 1), the volume of ambient air mixed into the plume for a time step of 1 second corresponds to

$$\Delta V = 2\pi \cdot 10\,\mathrm{m}^2\,\mathrm{s}^{-1} \cdot 10\,\mathrm{m\,s}^{-1} \cdot (1\,\mathrm{s})^2 \approx 6.3 \times 10^2\,\mathrm{m}^3 = 6.3 \times 10^8\,\mathrm{cm}^3 \tag{26}$$

When assuming again that this volume of air contains 40 ppb O_3, which corresponds to a concentration of $[O_3] \approx 1 \cdot 10^{12}\mathrm{cm}^{-3}$, the flow of O_3 into the plume is given by

$$F = [O_3] \cdot \frac{\Delta V}{\Delta t} \approx 6.3 \times 10^{20}\,\mathrm{s}^{-1}. \tag{27}$$

This corresponds well to the first value derived for the flow of O_3 molecules into the plume.

Now, to finally estimate the removal of O_3 trough reactive bromine chemistry the chemical reactions described in Sec. 2.3 come into play. As discussed in Sec. 2.3, the reactions 12, 13 and 14 are thought to be mainly responsible for the O_3 destruction. Considering the kinetics it becomes apparent, that the BrO self reaction limits the depletion of O_3. The destruction of O_3, which itself takes place due to the reaction with Br (see Reac. 12), can therefore be approximated with the rate of self reactions of BrO (Reac. 13 and 14),

$$\frac{d[O_3]}{dt} = k_{O_3+Br} \cdot [O_3] \cdot [Br] \approx 2 \cdot k_{BrO+BrO} \cdot [BrO]^2. \tag{28}$$

The factor two is needed since the self reaction of BrO produces two Br atoms, which in turn can react with two O_3 molecules.
When assuming typically measured BrO concentrations $[BrO] \approx 10^{10}\mathrm{cm}^{-3}$ and a reaction constant $k_{BrO+BrO} \approx 2.7 \times 10^{-12}\,\mathrm{cm}^3\mathrm{molec}^{-1}\mathrm{s}^{-1}$ Eqn. 28 yields an O_3 destruction rate of

$$\frac{d[O_3]}{dt} \approx 5.4 \times 10^8\,\mathrm{cm}^{-3}\,\mathrm{s}^{-1}. \tag{29}$$

By multiplying it with the volume of the inner plume one obtains the number of O_3 molecules destroyed by the reaction with bromine. Here, the assumption is included that the chemical reactions responsible for the O_3 depletion only proceed in the inner part of the plume. The inner volume can be calculated with

$$V = \pi \cdot (r - \Delta r)^2 \cdot \Delta s \approx 3 \times 10^{10}\,\mathrm{m}^3. \tag{30}$$

The total destruction rate of O_3 is then given by

$$R = \frac{d[O_3]}{dt} \cdot V \approx 1.6 \times 10^{19}\,\mathrm{s}^{-1} \ll 6.3 \times 10^{20}\,\mathrm{s}^{-1} < 1.25 \times 10^{21}\,\mathrm{s}^{-1}. \tag{31}$$

This calculation suggests that the assumption of a local O_3 depletion inside a plume, which is roughly 125 s old, is invalid through a contradiction. If local O_3 depletion is assumed, the flow into the plume exceeds the destruction rate by two orders of magnitude and therefore replenishes O_3 within one second to almost ambient levels. This implies that O_3 should be depleted by only 1% compared to ambient levels for this plume configuration. The assumption of local O_3 depletion through the assumed process within the plume is therefore invalid.

Another example with a different plume geometry corresponding to an older plume age (roughly 12500 s) is calculated based on the same approach as taken above. The start parameters as well as the results of this calculation are listed in Fig. 1 *right*. With these values the destruction equals the influx of O_3 therefore enabling the existence of a local O_3 hole.
Here, we assumed the BrO mixing ratios to be equal to the values assumed for example 1 and therefore neglected the dilution of the plume. Smaller BrO mixing ratios might therefore be expected and the assumed BrO mixing ratio should therefore be considered as an upper bound. When considering dilution, the BrO mixing ratios are two orders of magnitude lower since they scale anti proportionally with the square of the radius. This would then again lead to the result that the flow of O_3 into the plume is by 2 orders of magnitude larger than the destruction of O_3 inside the plume.

A slightly different perspective on the same approach would be to assume that for a local O_3 depletion in the plume the influx of O_3 should not exceed the bromine-catalysed destruction of O_3. Calculating the destruction therefore enables to estimate the influx of O_3 into the plume. From this then the concentration difference of O_3 inside and outside of the plume can be calculated. Assuming ambient mixing ratios of 40 ppb O_3 the concentration of O_3 inside, or rather the relative depletion compared to ambient levels can be estimated.

$$F \stackrel{!}{=} R \tag{32}$$

$$j \cdot A = R \tag{33}$$

$$K_t \cdot \frac{\Delta c}{\Delta r} \cdot A = R \tag{34}$$

$$\Rightarrow \Delta c = \frac{R \cdot \Delta r}{K_t \cdot A} = \frac{1.6 \times 10^{19}\,\mathrm{s^{-1}} \cdot 20\,\mathrm{m}}{10\,\mathrm{m^2 s^{-1}} \cdot 2.5 \times 10^{7}\,\mathrm{cm^2}} \tag{35}$$

$$\approx 1.3 \times 10^{10}\,\mathrm{cm^{-3}} \tag{36}$$

$$\Rightarrow \frac{\Delta c}{c_{\mathrm{O_3,ambient}}} = \frac{1.3 \times 10^{10}\,\mathrm{cm^{-3}}}{1 \times 10^{12}\,\mathrm{cm^{-3}}} = 1.3\% \tag{37}$$

The result is again that only a depletion on the order of 1% compared to ambient levels for this plume configuration should be expected. Here, the numerical results calculated in the first part were used.

From this calculation the question arises: "Is there an O_3 depletion in volcanic plumes?". This further underlines the need for more and in particular more reliable measurements of O_3 in volcanic plumes.

4 Instruments

A wide variety of measurement techniques for O_3 are available. CL, UV absorption as well as electrochemical monitors can be used to measure O_3 mixing ratios.

In this thesis a gas-phase CL O_3 monitor is characterised and compared to an UV absorption monitor, as these instruments are most commonly used for monitoring atmospheric O_3 and volcanic measurements.

4.1 Chemiluminescence ozone monitor

CL describes the emission of photons as the result of a chemical reaction.
As the name of a CL O_3 monitor already suggests its operation principle relies on the production of chemiluminescent species via a reaction with O_3. With the measurement of the thus emitted photons conclusions on the concentration of O_3 can be drawn.
In particular, gas-phase reactions of O_3 with olefins are known to yield the emission of photons. Arguably the most prominent option for a CL monitor is the gas-phase ozonolysis of ethylene (C_2H_4). However, also CL monitors relying on different reactions are available. For instance, an alternative is another gas-phase CL monitor exploiting the CL produced by the reaction of O_3 with NO. Additionally, dry CL instruments as well as wet CL instruments can be used, which make use of the reaction of O_3 with organic dyes in the condensed phase (Zahn et al., 2012).

In this thesis a custom-build CL O_3 monitor provided by MLW Messtechnik für Luft- und Wassereinhaltung, Florstadt is studied. It is a gas-phase CL monitor relying on the reaction of O_3 with C_2H_4. It is adapted from the Bendix CL O_3 monitor model 8002, i.e. the core of the monitor, the reaction cell with the photomultiplier tube (PMT) as well as the electronics needed for its operation, were taken over from the old unit. For a description of the original device see the Bendix manual "Bedienungshandbuch - Ozon Analysator Modell 8002" (UPK). A more in depth description of the current type of monitor can be found in the operation manual "Bedienungsanleitung in Kurzform; Immissions Ozonmonitor für Messungen in Vulkan Rauchfahnen (Prototyp 1)" (Aletter, 2020).

4.1.1 Configuration/device description

The CL O_3 monitor described here is a portable, backpack-sized (40 x 30 x 18.7 cm) instrument. It weighs approx. 10 kg and has an average power consumption of 30 W. Higher values have to be anticipated during the warm up phase of the monitor, during which the Peltier elements start cooling the PMT. The power consumption increases with measurement time as the monitor continually heats up and hence requires more cooling by the Peltier elements. The monitor can be operated either with a power bank (12 V/20 A h $\rightarrow$ 2 h, holders for two power banks) or an external power adaptor. In Fig. 2 the device configuration can be seen.

The main part of the instrument is the measurement cell and the PMT with its electronic unit in the rear part. To reduce contamination of the measurement cell, by e.g. dust, ash, or vapour droplets, a Teflon aerosol filter is placed at the air inlet through which ambient air is introduced into the measurement cell with a flow rate of $\sim 8.3\,\mathrm{ml \cdot s^{-1}}$.

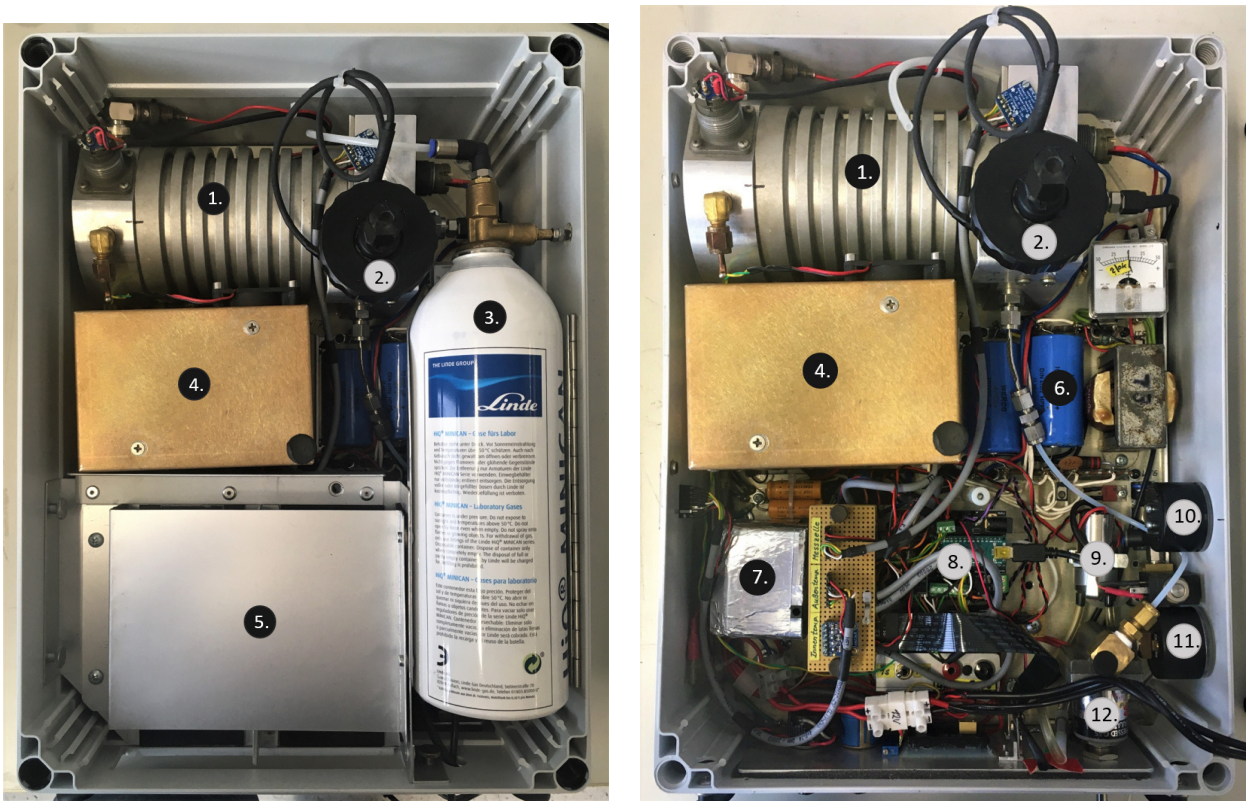

Figure 2: Configuration of the CL O_3 monitor.
left: View from above with intermediate frame. *right:* View from above without intermediate frame.
1. PMT and measurement cell; 2. Air inlet with Teflon aerosol filter; 3. C_2H_4 Minican; 4. Bendix plug in boards; 5. power bank compartment; 6. Temperature regulation; 7. inverter; 8. Arduino unit; 9. pump; 10. manometer (bottle pressure); 11. manometer (operation pressure); 12. pressure reducer

As C_2H_4 source minicans are used with a volume of 1 L and 12 bar initial pressure.
The minican is connected to a pressure regulator providing a working (over-)pressure of 12 psi (0.83 bar) and a capillary regulating the flow to $\sim 0.2\,\mathrm{ml \cdot s^{-1}}$ before C_2H_4 enters the measurement cell. A minican can be used for approx. 8 h.
A carbon-vane pump behind the measurement cell, in conjunction with the capillaries, ensures the desired total flow rate of approx. $8.5\,\mathrm{ml \cdot s^{-1}}$ or $30\,\mathrm{L \cdot h^{-1}}$ for the C_2H_4 and ambient air mixture.

The measurement cell has a capacity of approx. 12 ml (assuming a radius of 2 cm and a thickness of 1 cm). This leads to a flushing time of roughly 1.4 s (for a flow of $8.5\,\mathrm{ml \cdot s^{-1}}$). Within the measurement cell the reaction of O_3 with C_2H_4 takes place. Directly adjacent to the measurement cell is the PMT detecting the emitted photons. The electronic signal of the PMT, which is proportional to the number of emitted photons, is then read out, logged and saved to an SD card using an Ardunio Nano. With two potentiometers, which can be set with two knobs at the front panel, the zero value and the range can be adjusted.

To monitor the instruments potential dependencies on environmental changes the monitor is equipped with three temperature, pressure, and humidity sensors. One is attached to the outside of the instrument monitoring the outside conditions, one placed inside the instrument monitoring the inside conditions and the last one is attached to the housing of the PMT. During measurements the PMT housing heats up due to the waste heat of

the Peltier elements which cool the PMT.

The time is recorded using a real time clock (RTC). The RTC can be set with the upload of code on the Arduino and has a battery so the set time is not lost even when the instrument is switched of. As the upload of the code to the Arduino can be timed with only limited precision, the RTC can only be set this precise. Additionally, the built-in function of the Arduino to log the milliseconds since power on is used.

Furthermore, the supply voltage is saved as this might provide insight into possible errors and facilitate their rectification. Additional information on the instruments configuration such as wiring diagrams can be found in the appendix 9.

4.1.2 Theory of operation

From the reaction of O_3 with C_2H_4 a great diversity of products can be observed, among them excited species leading to the emission of photons on their de-excitation. The emitted photons are measured with the PMT directly connected to the measurement cell.

The emission of photons can mainly be attributed to formaldehyde fluorescence (electronically excited formaldehyde ($HCHO^*$)) as well as to $OH^\dagger$ Meinel band emissions (Finlayson et al., 1974). Here, electronically excited species are denoted with $*$, vibrationally excited species with $\dagger$. The emission spectrum of the reaction and the spectrum of formaldehyde fluorescence excited by tesla coil discharge are shown in Fig. 3 (Finlayson et al., 1974).

In kinetic studies of the reaction the emission intensities have been found to be first order in the O_3 concentration as both emitting species ($HCHO^*$, $OH^\dagger$) show a reaction order of approx. 1 for pseudo first-order conditions (Finlayson et al., 1974). Pseudo first-order conditions apply also in the configuration of the CL O_3 monitor as C_2H_4 is available in excess during the reaction and thus eliminates the dependence of the reaction rate on the C_2H_4 concentration (stays relatively constant during the reaction).
As the light intensity and therefore the number of emitted photons is proportional to the mixing ratio of O_3 the electronic signal of the PMT is also proportional to the mixing ratio of O_3. For a pressure of 4.6 Torr (6.1 mbar) 1×10^{-4} photons $\cdot$ mol^{-1}s^{-1} for both emitting species were measured (Finlayson et al., 1974).

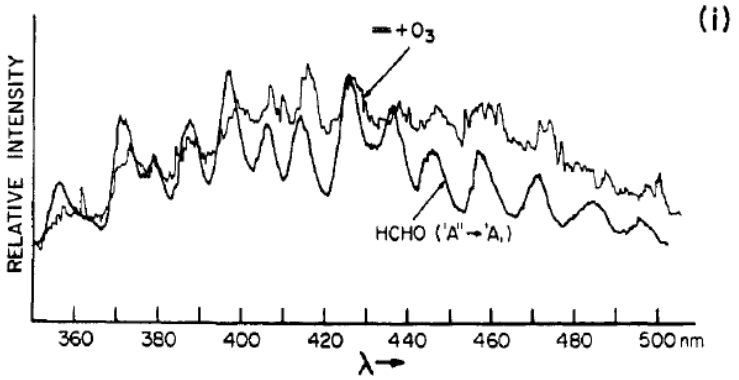

Figure 3: Chemiluminescent emission spectra from the reaction of O_3 with C_2H_4 at 4.5 Torr. Additionally the emission spectrum of electronically excited formaldehyde is plotted for comparison. Source: Finlayson et al. (1974)

Usually, in order to explain the reactions the O'Neal-Blumenstein hydrogen abstraction modification (O'Neal and Blumstein, 1973) in conjunction with the Criegee mechanism is used (Barnes and McGrath, 1986). The general mechanism is shown in the following scheme (adapted from O'Neal and Blumstein (1973); Barnes and McGrath (1986); Finlayson et al. (1974); Olzmann et al. (1997), picture from Kleindienst et al. (1993)). In this scheme the two reaction pathways for the reaction of O_3 and C_2H_4 are shown.

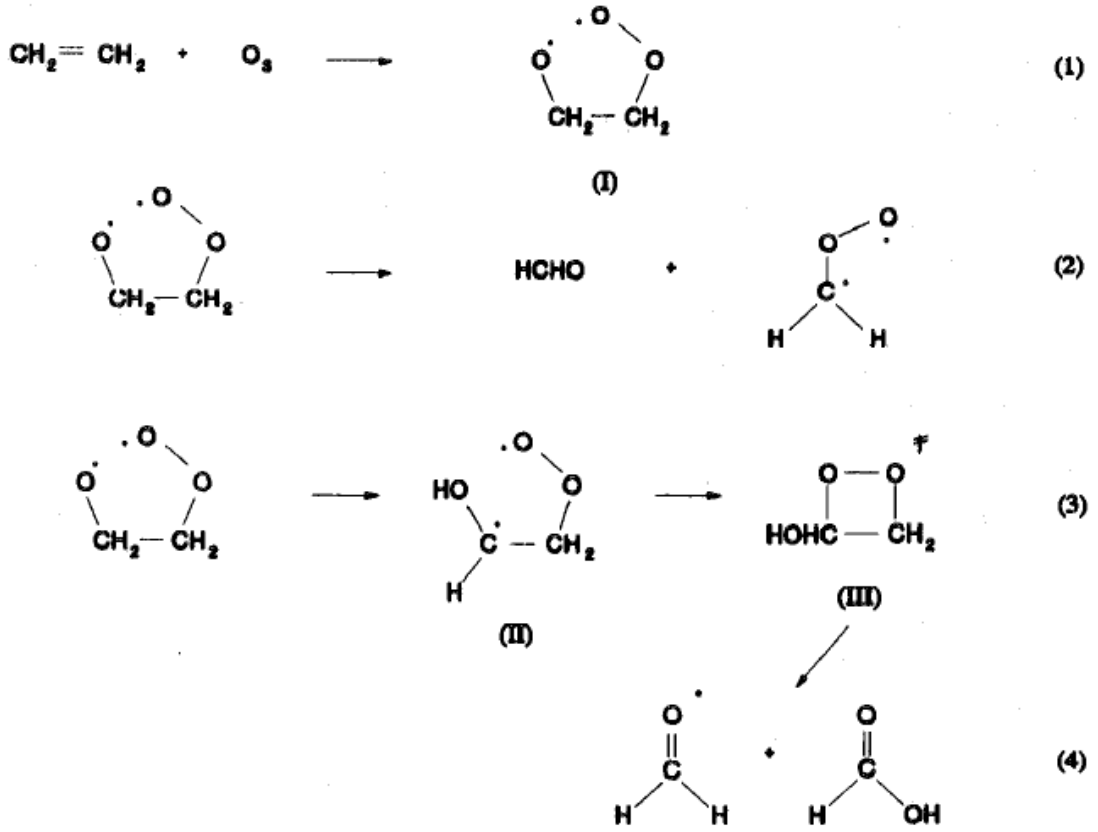

Figure 4: Schematic of the reaction of O_3 with C_2H_4. The first mechanism (reaction 2), called the Criegee split, results in the excited Criegee intermediate. The second mechanism (reactions 3 and 4) show the α hydrogen abstraction modification, which results in the production of electronically excited formaldehyde HCHO*. Source: Kleindienst et al. (1993)

In the initial reaction (1) (Fig. 4) the primary ozonide is formed which can react in several ways:
Reaction (2) (Fig. 4) shows the Criegee split, where HCHO and the excited Criegee intermediate (CH_2OO^*) are formed. Further reaction pathways of the Criegee intermediate might explain the $OH^\dagger$ Meinel band emissions via the production of atomic hydrogen (H). The H atoms then react in the following way

$$H + O_3 \longrightarrow OH + O_2 \cdot \tag{38}$$

Reactions (3) and (4) (Fig. 4) show the α hydrogen abstraction (as proposed by O'Neal and Blumstein (1973)) which is thought to explain $HCHO^*$. Additionally, formic acid (HCOOH) is formed.

Important parameters influencing the strength of the signal, are the reaction rate in conjunction with the flushing duration t_{flush} of the measurement cell since these two parameters determine how many O_3 molecules react and with that, determine the number of produced photons. The reaction kinetics are given by (Atkinson et al., 2006),

$$O_3 + C_2H_4 \longrightarrow \text{products}, \tag{39}$$

$$\frac{d[O_3]}{dt} = -k(T)[O_3][C_2H_4], \tag{40}$$

$$\text{with} \qquad k(T) = 9.1 \cdot 10^{-15} \exp\left(-\frac{2580}{T}\right). \tag{41}$$

To obtain the total number of reacted O_3 molecules the differential equation 40 is solved for the concentration of O_3. Since C_2H_4 is available in excess its concentration is assumed to be constant during the course of the reaction which significantly eases solving the differential equation. Separation of variables, integration and finally solving for $[O_3]$ yields

$$[O_3](t) = [O_3]_0 \cdot \exp\big(-k(T) \cdot [C_2H_4]_0 \cdot t\big). \tag{42}$$

With this the concentration at time t_{flush} is calculated and then subtracted from the starting concentration $[O_3]_0$ to give the number of reacted O_3 molecules,

$$\text{reacted } O_3 = [O_3]_0 \Big(1 - \exp\big(-k(T) \cdot [C_2H_4]_0 \cdot t_{flush}\big)\Big). \tag{43}$$

For O_3 mixing ratios of 40 ppb at a temperature $T = 290\,\text{K} \approx 17\,^\circ\text{C}$ approx. 66% of the initial O_3 have reacted at the time t_{flush}.

From Eqn. 43 one sees that the number of reacted O_3 molecules and therefore the signal strength is dependent on the temperature T. However, also other temperature dependent parameters influence the CL monitors signal, so a temperature dependence of the signal can have a a number of reasons. These include:

1. temperature dependence of the dark current of the PMT, which can be measured when no photons enter the PMT
2. temperature dependence of the electronic components
3. changes in the density of air and with it in the concentrations of trace gases
4. temperature dependence of the rate constant of the reaction generating the chemiluminescent species (i.e. the reaction $O_3 + C_2H_4 \longrightarrow$ products)
5. change in quenching of the chemiluminescent species with temperature

The first two dependencies are of technical nature and we will assume that the temperature dependence of the electronic components is of minor importance. The dark current of the PMT is mostly caused by indispensable thermionic emission of electrons. The magnitude of these effects depend on material characteristics and on temperature (Baicker).

To minimize its effect the PMT is cooled by Peltier elements to a temperature of roughly 5 °C, which also ensures long-time stability of the measurement (UPK). The temperature dependence of these technical parameters is studied in experiments (see Sec. 5.1.3).
Bullet points 3. - 5. are the temperature dependence of the chemical reaction itself. The temperature dependence of the quenching of the chemiluminescent species is not known. Therefore, in the following only the change in signal with temperature arising from the concentration and the rate constant (bullet points 3. and 4.) is considered. The temperature dependence of the concentration can be acquired by considering the ideal gas law (Eqn. 18)

$$c_i = \frac{\nu_i \cdot N_A}{V_{air}} = \frac{V_i}{V_{air}} \cdot \frac{p \cdot N_A}{RT} = x_{V,i} \cdot \frac{p \cdot N_A}{RT}, \tag{44}$$

where i denotes the species considered.
A temperature increase therefore leads to an increase of the reaction constant k but simultaneously to a lower concentration. In Tab. 4 the total number of reacted O_3 molecules as well as the starting concentrations of the reactants, the reaction constant and the resulting reaction rate are listed for two temperatures.
From these values one notices that the increase in signal due to a rise in temperature of 20 °C is slightly more pronounced for higher O_3 mixing ratios.

		~ 40 ppb O_3		~ 150 ppb O_3	
		$T = 290$ K	$T = 310$ K	$T = 290$ K	$T = 310$ K
$[O_3]_0$	$[cm^{-3}]$	9.8×10^{11}	9.2×10^{11}	3.7×10^{12}	3.4×10^{12}
$[C_2H_4]_0$	$[cm^{-3}]$	5.8×10^{17}	5.4×10^{17}	5.8×10^{17}	5.4×10^{17}
$k(T)$	$[cm^3\,s^{-1}]$	1.24×10^{-18}	2.2×10^{-18}	1.24×10^{-18}	2.2×10^{-18}
$[O_3](t_{flush})$	$[cm^{-3}]$	3.3×10^{11}	1.5×10^{11}	1.3×10^{12}	5.7×10^{11}
reacted O_3	$[cm^{-3}]$	6.5×10^{11}	7.7×10^{11}	2.4×10^{12}	2.9×10^{12}
		66.3%	83.6%	64.8%	85.3%
relative increase		-	18.5%	-	20.8%

Table 4: Rough estimations on the temperature dependence of the signal. The concentration of reacted O_3 molecules is listed as it is proportional to the produced photons. Additionally the relative increases for the temperature increase of 20 °C is calculated.

4.2 UV absorption ozone monitor

As UV absorption instruments have proven to be a good choice of instrument, especially in air quality monitoring networks, they are presumably the most commonly used O_3 monitors. This can be attributed to their easy usage as no reagent gases or solutions are needed for their operation and to their low maintenance (Williams et al., 2006). Usually, they can be manufactured as lightweight, handheld devices, facilitating their application also in non stationary measurements. For these reasons an UV absorption monitor, namely, the 2B Technologies Personal Ozone Monitor (POM), as comparison instrument is used for this thesis.

The POM is a small (10 x 8 x 3 cm) and portable O_3 monitor. It weighs roughly 350 g and has a low power consumption of approx. 3 W. Additionally to the O_3 mixing ratios the instrument measures the cell temperature, the pressure and the voltage of the photodiode as well as GPS coordinates (latitude, longitude, altitude, quality). A more detailed description of the instrument can be found in the operation manual (POM, 2020).

4.2.1 Theory of operation

UV absorption monitors make use of the characteristic properties of the O_3 molecule to absorb electromagnetic waves strongly at a wavelength of 254 nm. This absorption can be attributed to the so called Hartley band, which extends from 200 nm to 310 nm. By measuring the attenuation of light at 254 nm along a well defined path the O_3 concentration can be determined using Beer-Lambert law,

$$\frac{I}{I_0} = exp\big(-\sigma \cdot L \cdot [\mathrm{O_3}]\big) \tag{45}$$

where σ is the O_3 absorption cross section ($\sigma \approx 1 \times 10^{17}$ at 254 nm), L is the optical path length and $[O_3]$ the concentration of O_3 (Williams et al., 2006).
The optical density is then given by

$$\ln\left(\frac{I}{I_0}\right) = -\sigma \cdot L \cdot [\mathrm{O_3}], \tag{46}$$

and takes on values of typically approx. 1×10^{-4}. Eqn. 45 (and with it Eqn. 46) can be derived from the more general form of Beer-Lambert law if the cross section σ as well as the density of the considered medium is constant over the considered path.

In Fig. 5 *right* a schematic diagram of the POM can be seen.
The main component of the instrument is its u-shaped absorption cell and the low-pressure mercury (Hg) lamp with a principle wavelength of 254 nm. The light emitted from the Hg lamp is transmitted to the other end of the cell via two mirrors. There, a photo diode with a built in filter centred on 254 nm detects it. A pump behind the absorption cell draws in ambient air into the absorption cell. The air is either drawn in directly into the cell or first passes an O_3 scrubber, depending on the setting of the solenoid valve. These two settings allow for the measurement of the two intensities:
I_0, the intensity of light when O_3 is removed and I, the intensity when the air did not pass the O_3 scrubber.

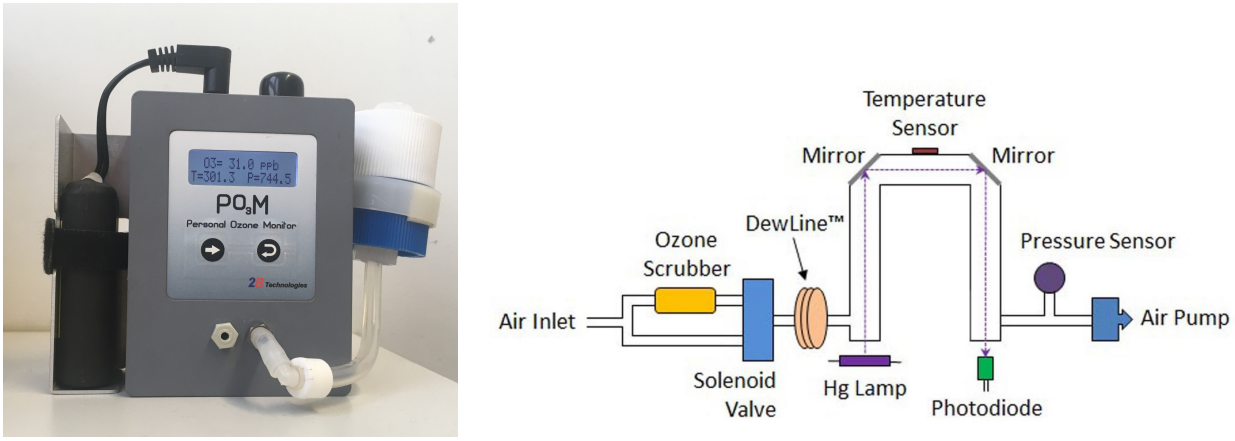

Figure 5: Photo (*left*) and schematic configuration (*right*) of the POM. Air is drawn into the air inlet and reaches then the u-shaped absorption cell, either directly or first passing an O_3 scrubber to remove all O_3. The pump drawing in the air is located behind the absorption cell. The light of the Hg lamp is directed at the photodiode via two mirrors. Source: Manual POM (2020)

With Eqn. 45 the concentration of O_3 can be calculated via

$$[O_3] = \frac{1}{\sigma \cdot L} \cdot ln\left(\frac{I}{I_0}\right), \tag{47}$$

where L is the length of the absorption cell.

With the ideal gas law 18 the total number of air molecules N_{tot} can be determined using the temperature T and the pressure p

$$N_{\text{tot}} = \frac{pVN_A}{RT}. \tag{48}$$

The total number of O_3 molecules can easily be derived from the concentration

$$N_{O_3} = [O_3] \cdot V \tag{49}$$

Using Eqns. 47, 48 and 49 the mixing ratio can be calculated via

$$x_{V,O_3} = \frac{V_{O_3}}{V_{\text{tot}}} = \frac{N_{O_3}}{N_{\text{tot}}} = \frac{R \cdot T}{N_A \cdot p \cdot L \cdot \sigma} \cdot ln\left(\frac{I}{I_0}\right). \tag{50}$$

As this measurement technique is an absolute method, ideally no external calibration is needed. However, non-linearities may occur and result in measurement errors. Especially, after frequent operation of the instrument a calibration is needed from time to time.

4.2.2 Reliability of measurements

As mentioned above, UV absorption instruments are most commonly used for monitoring ambient O_3. It is however known, that there are some positive interferences which might adulterate O_3 measurements under certain conditions. This interference is mainly caused by absorption at 254 nm of other species than O_3, e.g. volatile organic carbon species and other trace gases such as SO_2. Some studies, such as an ambient monitoring and smog chamber study by Leston et al. (2005), show significantly increased O_3 measurements from UV absorption monitors compared to CL monitors. There is also some positive interference reported from fine aerosols ($< 0.2\,\mu m$ diameter) and aerosols (2.5 µm diameter) (Williams et al., 2006, and references therein).

Other studies, however, conclude that there is no significant interference due to absorption of other species than O_3 under 'normal' atmospheric conditions. This is the result of a study from Kleindienst et al. (1993). They show that interference is negligible with the only exception being highly polluted environments. Williams et al. (2006) conducted measurements covering a wide range of sampling conditions, including environments with significant ambient concentrations of potentially interfering volatile organic carbon species. They conclude that no significant interference can be seen in the UV absorption measurements when compared to a CL instrument.

The studies above indicate that monitoring O_3 in urban and also industrial locations can therefore be reliably done using UV absorption monitors, even when there is some pollution.
When measuring O_3 in volcanic plumes the situation is different. Volcanic gases contain high mixing ratios of SO_2 compared to ambient air. This poses a problem since UV absorption measurements of O_3 are known to exhibit positive interference from SO_2.

In Fig. 6 the cross sections of O_3 and SO_2 are illustrated. At the emitting wavelength of mercury - at 254 nm - the cross section of O_3 exceeds the cross section of SO_2 by a factor of roughly 100, thus making the UV absorption monitor approx. 100 times more sensitive to O_3 compared to SO_2. Usually, the mixing ratios of SO_2 do not exceed a few ppb and O_3 mixing ratios take on values of 40 ppb. The resulting increase in signal from SO_2 is significantly smaller than 1% of the signal from O_3. Therefore, the effect of SO_2 interference on O_3 measurements under these conditions is negligible.

However, volcanic gases contain high amounts of SO_2 with mixing ratios reaching up to several tens of ppm and thus exceeding O_3 mixing ratios by factors of 1000 or more. This causes an interference signal from SO_2 of several 10 to 100 ppb and therefore reliable O_3 measurements in volcanic plumes are strongly impeded.

This problem can be resolved by data post processing or introducing SO_2 filtering techniques, for example through the use of CrO_3 scrubbers. Both approaches have been used in previous studies (post processing: Kelly et al. (2013), scrubber: Surl et al. (2015), Vance et al. (2010)) but entail further problems. For instance, humidity dependencies have to be considered when using filtering techniques. If the positive interference from SO_2 is to be removed via post processing additional measurements of SO_2 have to be done in parallel. Thus, time synchronisation issues are introduced. Also, there is no universal conversion factor to obtain the effect of the measured SO_2 mixing ratios on O_3 measurements since every UV monitor reacts slightly differently to SO_2. Therefore, the reaction of the UV absorption monitor towards SO_2 has to be established.
Applying either one of these techniques is laborious and can be a further error source.

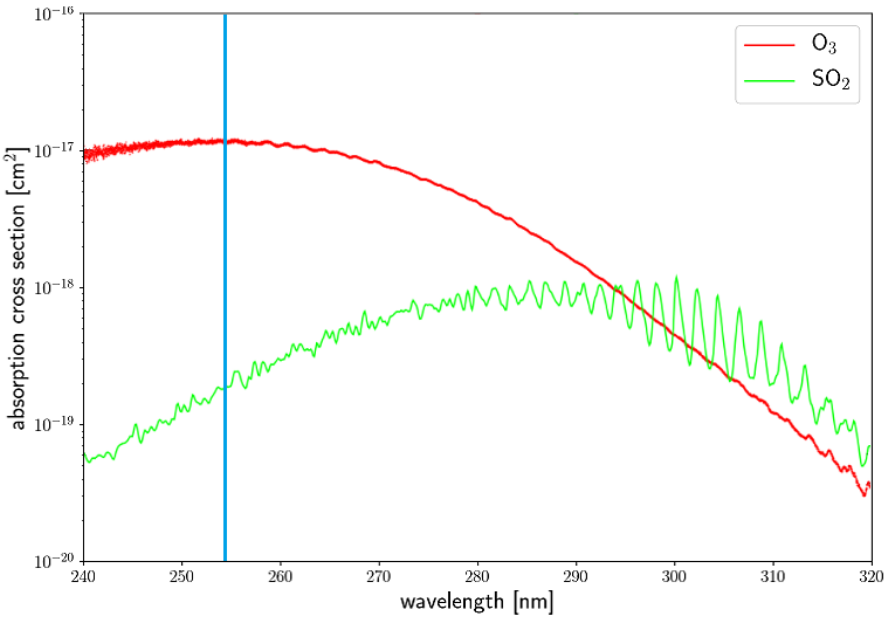

Figure 6: Comparison of cross sections of O_3 (red) and SO_2 (green). Additionally, the main emission wavelength of mercury (Hg) at 254 nm is marked (blue). The cross sections of the two species deviate by a factor of roughly 100 at 254 nm, causing a 100 times higher sensitivity to O_3 than to SO_2. Source: adapted from Herr (2011)

5 Characterisation

5.1 Chemiluminescence ozone monitor

5.1.1 Calibration

The CL O_3 monitor is calibrated using an O_3 generator. This O_3 generator has two settings which can be used for calibration: zero gas containing 0 ppb O_3 and test gas with 150 ppb O_3. Test gas containing higher values of O_3 mixing ratios are possible, these settings do, however, not produce calibrated test gas.

As the CL monitor requires about 10 to 10 min, depending on ambient temperature, to warm up after power on, this data is usually discarded. In addition and independent of the remaining warm up phase, the first minutes after power on are dominated by a steep decline in the O_3 signal starting from about several hundred ppb of O_3. Roughly 2-3 min after power on the O_3 signal then reaches the zero line. This phenomenon can with great certainty be traced back to the initiation of the PMT, in particular its cooling system.

Once the CL monitor has warmed up the C_2H_4 minican is opened and the zero gas from the O_3 generator is passed trough the instrument. After a stabilisation period of roughly 10 min the O_3 generator is switched to 150 ppb. This procedure, switching the O_3 generators settings between 0 ppb and 150 ppb, is repeated several times. For the calibration the mean values and the standard deviations of the recorded data are calculated for each of the settings of the O_3 generator i.e. for 0 ppb and 150 ppb of O_3. These values are then used to obtain the actual mixing ratios of O_3 for the following measurements of ambient O_3 through the following linear relationship,

$$x_{\text{abs}} = (x_{\text{meas}} - v_{0\text{ppb}}) \cdot \frac{150}{v_{150\text{ppb}} - v_{0\text{ppb}}}. \tag{51}$$

Here x_{meas} denotes the measured mixing ratio, $v_{0\text{ppb}}$ is the mean value for 0 ppb, $v_{150\text{ppb}}$ the mean value for 150 ppb obtained from the calibration.

Via the 'zero' and 'span' potentiometers, which can be adjusted with two knobs at the front panel, the measured values, which are also displayed on the front-panel display, can be set accordingly during the calibration process. This serves as a useful direct feedback during measurements.

One problem which arose is the drift which occurred between different calibration procedures. Without readjusting the potentiometers on the front panel, the calibrations differed in the measured values of 0 ppb and 150 ppb O_3.
In Tab. 5 the values for all calibrations are listed. As these changes might be attributed to changes in the ambient conditions the mean values of the ambient conditions are summarised in Tab. 5. These values for temperature, pressure and humidity are obtained by averaging over the entire measurement duration.

The first calibration was carried out the day before the first field measurement. The values obtained from this calibration were then used as reference values for the following calibrations.

	date	description	$v_{0\text{ppb}}$	deviation	$v_{150\text{ppb}}$	$v_{150\text{ppb}}$-$v_{0\text{ppb}}$	deviation	temperature [°C]	pressure [hPa]	humidity [%]
1.	30.09	before 1. field measurement	200.1 ± 1.0	0	349.5 ± 1.9	149.4 ± 2.1	0	23.3 ± 1.8	925 ± 0.1	54 ± 5
2.	03.10	after 2. field measurement	197.3 ± 0.9	2.8 (2.1σ)	338.7 ± 1.7	141.4 ± 1.9	-8 (2.8σ)	24.7 ± 2.1	923.4 ± 0.3	62 ± 6
3.	05.10	new aerosol filter	203.8 ± 0.8	+3.7 (2.9σ)	328.1 ± 1.8	124.3 ± 2	-25.1 (8.7σ)	31.5 ± 3.2	925.8 ± 0.3	40 ± 7
4.	06.10		200.1 ± 0.7	0	333.2 ± 1.7	133.1 ± 1.8	16.3 (5.9 σ)	24.7 ± 2.0	928.7 ± 0.2	48 ± 7
5.	08.10	after 3. field measurement	200.5 ± 0.6	+0.4 (0.3σ)	332.2 ± 1.6	131.7 ± 1.7	-17.7 (6.6σ)	22.4 ± 1.5	931.9 ± 0.1	49 ± 6
6.	09.10		200.1 ± 0.5	0	335.6 ± 1.5	135.5 ± 1.6	-13.9 (5.3 σ)	21.0 ± 1.4	933.2 ± 0.1	46 ± 6
7.	14.10	at institute	200.0 ± 0.6	-0.1 (0.1σ)	353.4 ± 1.7	153.4 ± 1.8	+4 (1.4σ)	22.8 ± 1.2	1000.9 ± 0.1	36.2 ± 2.5
8.	23.10		200.8 ± 0.7	+0.7 (0.6σ)	353.1 ± 1.6	152.3 ± 1.7	+2.9 (1.1σ)	24.6 ± 1.6	1000.3 ± 0.1	45.6 ± 3.8
9.	23.10	shaking instrument	201.6 ± 0.7	+1.5(1.3 σ)	356.3 ± 1.8	154.7 ± 1.9	+5.3 (1.9σ)	26.8 ± 0.8	1000.3 ± 0.1	41.1 ± 1.6
10.	05.11		200.9 ± 0.7	+0.8 (0.6σ)	363.4 ± 1.7	162.5 ± 1.8	+13.3 (4.8σ)	30.2 ± 1.8	1022.4 ± 0.1	20 ± 2
11.	13.11		200.1 ± 0.6	0	359.6 ± 1.5	159.5 ± 1.6	+10.1 (3.8 σ)	24.2 ± 1.5	1000.3 ± 0.1	38.1 ± 3
12.	04.12		201.8 ± 0.4	+1.7 (1.6σ)	358.5 ± 1.5	156.7 ± 1.6	+7.3 (2.8σ)	23.1 ± 0.5	976.8 ± 0.1	37.7 ± 3.4
13.	07.12		201.9 ± 0.8	+1.8 (1.4σ)	362.8 ± 1.7	160.9 ± 1.9	+11.5 (4.1σ)	23.1 ± 1.9	988.5 ± 0.2	31.5 ± 4.3
14.	07.12		202.3 ± 0.5	+2.2 (2σ)	364.7 ± 1.7	162.4 ± 1.8	+13.0 (4.7σ)	27.4 ± 0.9	988.73 ± 0.03	3.8 ± 2.8
15.	22.01		205.4 ± 1.4	+5.3 (3σ)	371.9 ± 1.4	166.5 ± 2	+17.1 (5.9σ)	29.3 ± 0.8	981.8 ± 0.2	20.6 ± 1.8
16.	25.01		200.5 ± 0.5	+0.4(0.4 σ)	374.4 ± 1.2	173.9 ± 1.3	+24.5 (9.9σ)	21.5 ± 1.6	989.0 ± 0.5	25.9 ± 3.1
17.	20.02	new aerosol filter	201.6 ± 0.5	+1.5(1.3 σ)	370.9 ± 1.3	169.3 ± 1.4	+19.9 (7.9σ)	24.0 ± 2.0	1003.1 ± 0.3	29 ± 4

Table 5: Results for the calibrations. All values for 0 ppb and 150 ppb O_3 as well as their deviation from the expected value of the first calibration are listed. In addition the ambient conditions, temperature, pressure and humidity, averaged over the entire measurement duration, are shown.

Some of these changes in the calibration might indeed be traced back to differences in the ambient conditions, for instance, the significant jump which is observed between the 6. and 7. calibration. Here a change in the pressure occurred due to a change in altitude respective to sea level (Randazzo: ∼800 m above sea level, Heidelberg: ∼100 m above sea level).
However, for most calibrations no relation between the changes in signal and changes in the ambient conditions can be established. From this observed drift the need for regular calibrations for reliable measurements becomes apparent.
Another reason for the deviations might be attributed to the used O_3 generator producing unreliable mixing ratios of O_3.

In order to obtain the detection limit of the monitor the O_3 signal of periods during which zero gas of the O_3 generator is measured (or a scrubber is used) is averaged and the standard deviation is computed. Values of under 1 ppb are obtained for the standard deviation, which is then the 1 σ detection limit at an integration time of 1 s.

5.1.2 Time constant of the monitor

Another interesting parameter is the time needed for the monitor to adjust to a step change in the O_3 mixing ratio. Ideally, the monitor should react instantaneously but, for example, the flushing time of measurement cell and tubes in the monitor causes inertia towards sudden changes in O_3. In order to quantify the needed time for the monitor to adjust, either an increase (e.g. from 0 ppb to ambient O_3 mixing ratios (∼30 ppb) or to 150 ppb using the O_3 generator) or a decrease in the signal can be used which is approximated by an exponential function,

$$s(t) = a \cdot \left(1 - \exp\left(-\frac{(t-c)}{b}\right)\right) + d \qquad \text{for an increase and,} \tag{52}$$

$$s(t) = a \cdot \exp\left(-\frac{(t-c)}{b}\right) + d \qquad \text{for a decrease in signal.} \tag{53}$$

The time constant b of the exponential fit is used as a measure for this time.
However, the O_3 generator is not used to determine the monitor's time constant, since also the O_3 generator itself needs time to adjust and connecting tubes will further delay the change in signal. Instead, only the step changes which are created by removing or fixing a scrubber to the air inlet are used. In Fig. 7 *top*, an exemplary increase in the O_3 signal upon removing the scrubber from the air inlet with the corresponding exponential fit is shown. The time constant results in a value of $\sim$ 1.9 s. Very similar values are obtained when fitting other increases and decreases in the signals.
Even the decrease when switching the settings of the O_3 generator from 150 ppb to 0 ppb (here, the time lag caused by the O_3 generator itself is significantly smaller compared to the one which can be observed by switching from zero gas to 150 ppb) displays a value of $\sim$ 1.9 s. This decrease is shown in Fig. 7 *bottom*.

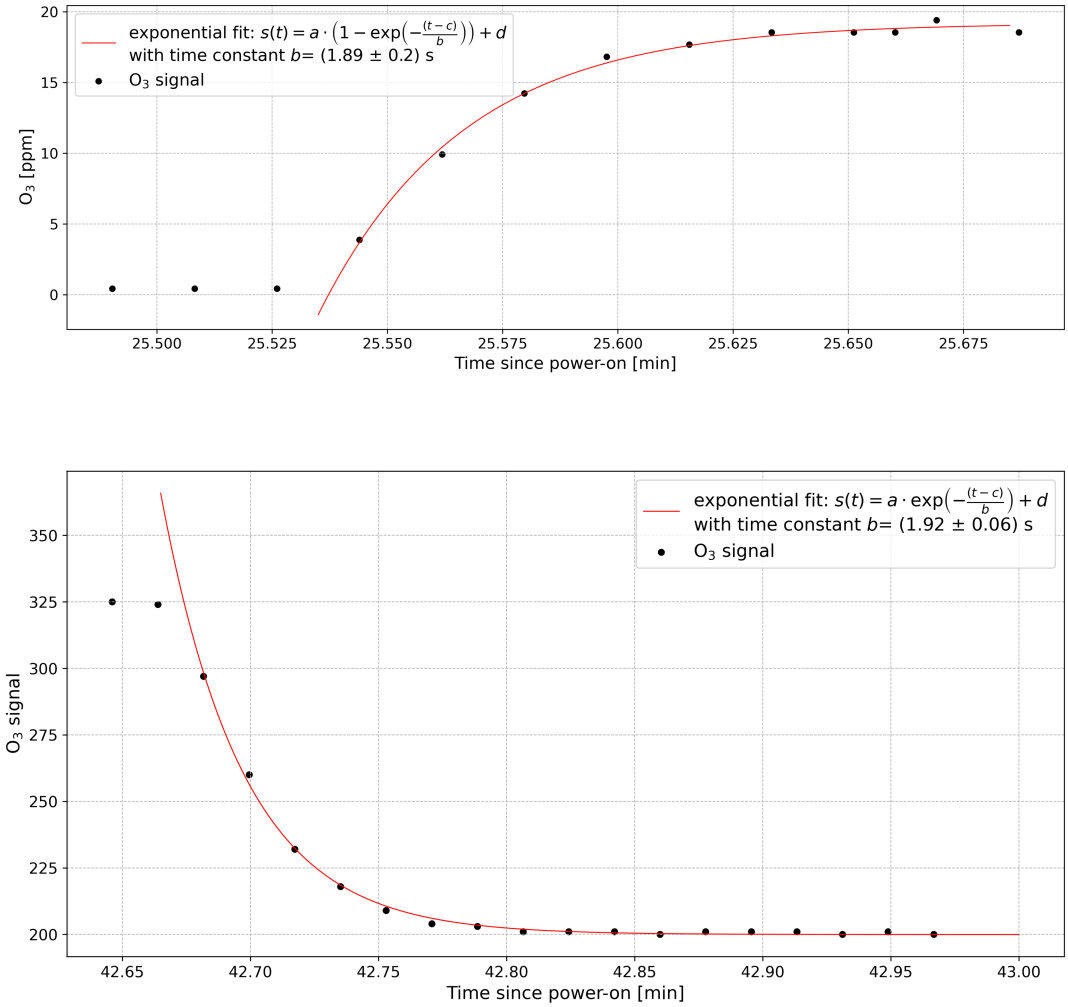

Figure 7: Reaction of the O_3 monitor to step changes in the O_3 concentrations are shown. To the measurement data (black) an exponential function is fitted (red). The time constant b, retrieved from the fit, is shown and is used as a measure for the monitor's time to react to a step changes in the O_3 mixing ratio.
top: Increase in the O_3 signal when the scrubber is removed. *bottom:* Decrease in the O_3 signal when the setting of the O_3 generator is switched from 150 ppb to zero gas.

5.1.3 Temperature dependence of the signal

In this section, the temperature dependence of signal measured with the CL monitor is studied. Studying and quantifying the temperature dependence is crucial as the CL monitor heats up during measurements due to the waste heat of the Peltier elements. In Sec. 4.1.2 the reasons for the possible temperature dependencies are listed.
For all following measurements, the temperature measured at the cell was used. Uncertainties in the analysis are introduced since not the actual temperature of the PMT or in the cell were used, which would be beneficial to correctly determine the temperature dependence.

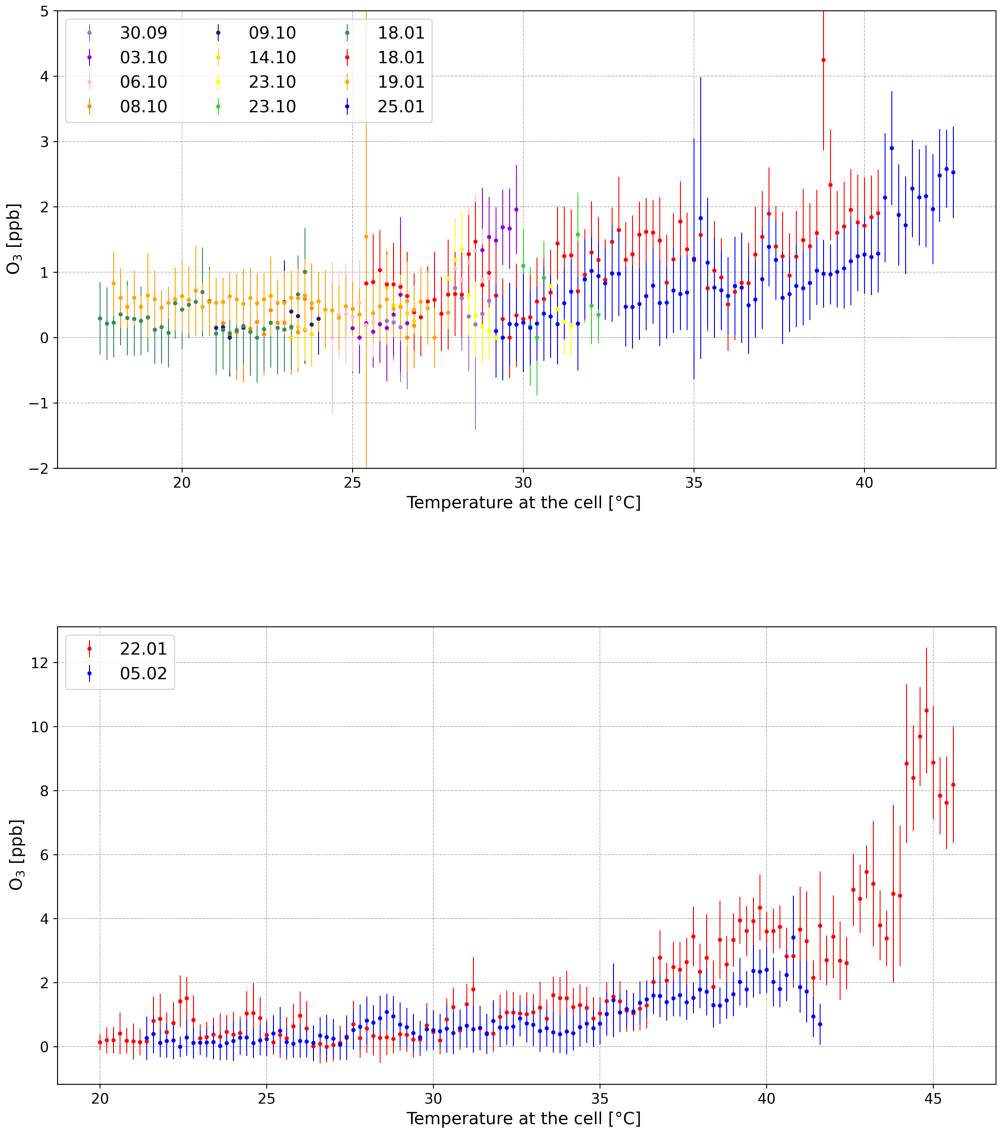

Figure 8: The signal of the dark current plotted against the temperature at the cell. The data points are obtained by averaging over temperature intervals of 0.2 °C, the error is given by the standard deviation. Different colours denote different measurements.
top: Measurements with power banks.
bottom: Measurements with external power adaptor.

Firstly, the temperature dependence of the dark current (combined with the effect of the temperature dependence of the electronic components) was studied. A measurement over several hours (approx. 4-6 h) was done without C_2H_4 and with a scrubber fixed to the air inlet to ensure the absence of both reactants. Thus no photons should entered the PMT. Over the course of the measurement, the PMT and with it the temperature at the measurement cell increases (as mentioned above). Several measurements with either power banks or the power adaptor were carried out.
Fig. 8 shows the means and standard deviations of the measurement values from within 0.2 °C temperature intervals for measurements using power banks (*top*) and the external power adaptor (*bottom*). Alongside measurements solely dedicated to quantify the

temperature dependence, also the calibrations of the instrument were evaluated.

When using power banks - this is the usual configuration during field measurements - the increase in signal arising from the dark current with temperature is insignificant. For temperatures at the cell between ∼17 °C and ∼40 °C only a slight increase in signal of under 2 ppb can be seen which corresponds to an increase of below 0.1 ppb · K^{-1}. Only single outliers exhibit values of over 2 ppb. For temperatures exceeding 40 °C the increase in signal becomes stronger with values reaching 3 ppb.
During measurements with the external power adaptor, however, a significant increase with temperature of up to 10 ppb can be observed for a temperature interval from ∼20 °C to ∼45 °C. However, less measurements using the power adaptor were made since usually power banks are used. An increase this high could only be observed during one single measurement. Furthermore, it has to be noted, that the increase in signal for temperatures exceeding ∼40 °C is more pronounced and not as steady as for smaller temperatures. For temperatures of under 40 °C, increases of 2 ppb and 4 ppb in the signal have been observed which are comparable to the increase with the power banks. Whether a stronger temperature dependence of the dark current should be anticipated, when using the external power adaptor compared to the power banks is therefore questionable and the high increase could also be considered as an outlier.

Additionally to the temperature dependence of the dark current, the temperature dependence of the reaction has to be considered. In Sec. 4.1.2 this temperature dependence is explained in more detail.
Analogous to the above explained experiment, the signal for a constant input of 150 ppb O_3 (from the O_3 generator) and the temperature at the cell over several hours were recorded. Here as well, calibrations, in particular their periods during which 150 ppb was measured, and the same processing of data were used.

In Fig. 9 three measurements of the temperature dependence of the signal for 150 ppb are presented. The first two measurements show a similar structure, where for the entire duration of the measurement the signal increases linearly with temperature. The slopes of the increase do, however, deviate significantly from another with approx. 0.6 ppb · K^{-1} for the measurement carried out on the 28th January 2021 and 1.4 ppb · K^{-1} for the measurement of the 5th February 2021. The slopes were obtained by fitting linear functions to the data. The third measurement shown, carried out on the 20th February 2021, at first exhibits a very similar increase to the measurement of the 28th January. Then however, the increase stagnates until temperatures of approx. 42 °C are reached where at first again a linear increase is observed which then does not show a specific trend for temperatures approaching 45 °C.
These three measurements are shown as they are representative of the trends also seen in the data from the calibrations. Most measurements exhibited increases with values between the slopes shown here. The increase in signal of 1.4 ppb · K^{-1} can therefore be assumed to be a maximum value for the temperature dependence of the 150 ppb signal. When assuming a temperature increase of about 10 °C (usually temperature increases of around 10 °C are observed in measurements of approx. 1-2 h) an increase of ∼14 ppb can be expected, which corresponds to slightly under 10% of the 150 ppb calibration signal. Assuming an increase in temperature of 20 °C would then lead to an increase by approx. 20%. This corresponds rather well with the values obtained from the estimations of the temperature dependence of the reaction for 150 ppb O_3 in Sec. 4.1.2. Here, the number of reacted O_3 molecules was found to increase by 20% for a temperature interval of 20 °C (from 17 °C to 37 °C) and the increase can be approximated to be linear with temperature.

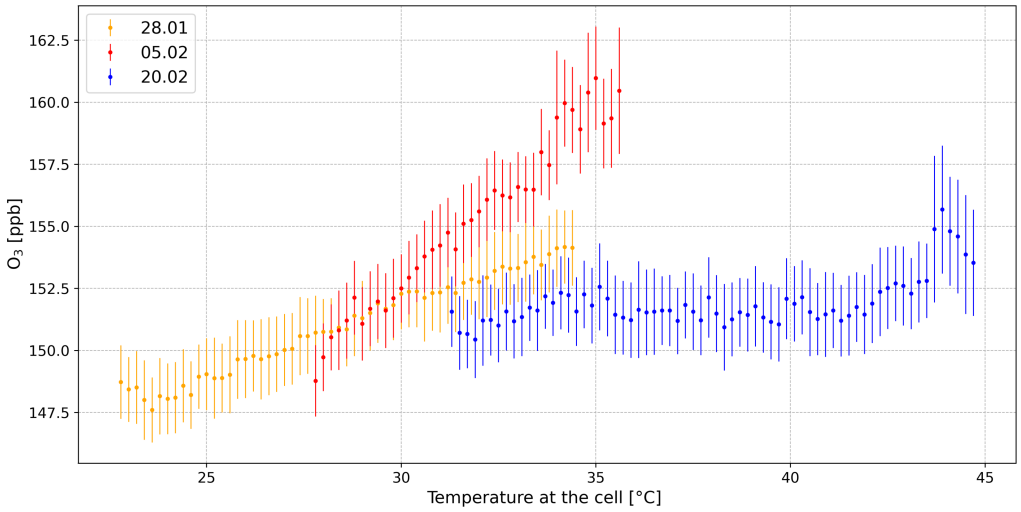

Figure 9: Dependence of the 150 ppb signal on temperature. The data points are obtained by averaging over temperature intervals of 0.2 °C, the error is given by the standard deviation. Different colours denote different measurements.

Ideally, this temperature dependence should be considered and corrected for in measurements. However, not all measurements show an increase with temperature this high as for example no temperature dependence at all for some periods or only an increase of $0.6\,\mathrm{ppb} \cdot \mathrm{K}^{-1}$ (which corresponds to only around 4% of the 150 ppb signal for a temperature rise of 10 °C) can be observed. There are still effects, such as the quenching of chemiluminescent species whose impact on the temperature dependence of the signal, are not determined yet. These uncertainties, also introduced through the approximation of the temperature in the cell with the temperature at the cell, impede the assessment of the observed temperature dependencies in relation to each other. Therefore, more measurements are needed to correctly determine the temperature dependence and then correct for it during measurements. The measurements in this thesis were corrected for the temperature dependence due to this observed variation and since the increase in signal should for most measurements stay below 10%.
What most measurements have in common is that for temperatures over 40 °C the signal does exhibit increasingly more outliers so the most reliable measurements can be done when the temperature at the cell does not exceed 40 °C. During the field measurements conducted here ambient temperatures were usually comparably low and the measurement duration was shorter (only around 1 h) so the temperature at the cell did not reach high values (e.g. only values of around 25 °C are reached). To prevent a strong heating of the monitor it might be beneficial to not conduct measurements in the direct sun. In order to prevent high temperatures at the cell in laboratory experiments the lid of the Cl monitor was not used. During these measurements the increase in temperature does usually not exceed 10 °C. Increases in the dark current for either power banks or the external power adaptor when the lid is kept open take on similar values of under 2 ppb, which further indicates the high increase in the signal of the dark current with the power adaptor to be an outlier.

5.1.4 Instrument overheating

In the beginning of the characterisation and calibration of the CL O_3 monitor the instrument overheated when measurements lasted several hours. Usually within the first two hours after power on the monitor operated as expected. Then, however, the PMT switched off and on roughly every five minutes causing the distinct drop in signal, which occurs at the beginning of every measurement (see Sec. 5.1.1) and can be attributed to the temperature regulation of the PMT. One of these measurements is shown in Fig. 10. The temperature at the cell still increases slightly after the first power-off of the PMT and then fluctuates roughly around 47 °C.

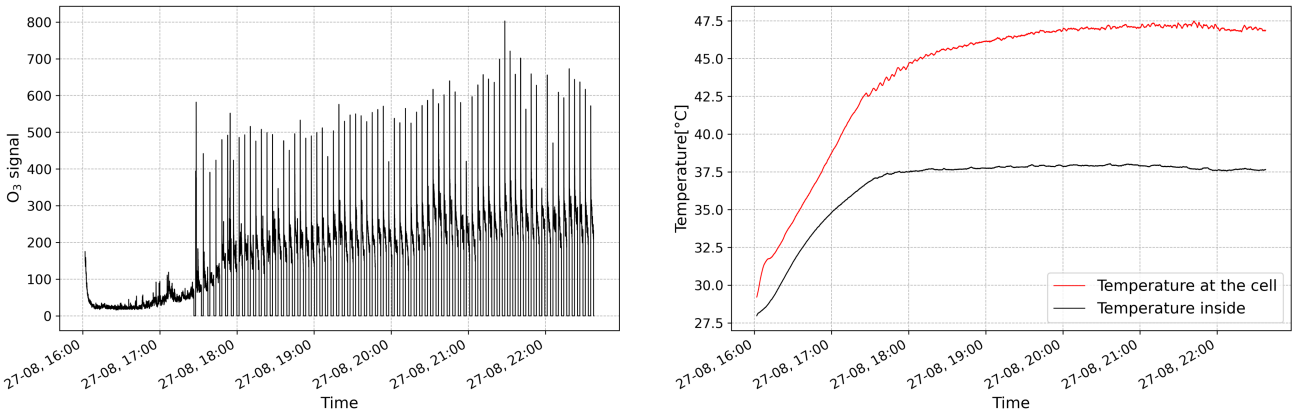

Figure 10: Time series of the O_3 signal (*left*) and the temperature (*right*) for one measurement during which the problem of overheating occurred. The PMT switches off and on, causing peaks in the O_3 signal. The temperature 'stabilises' at ~ 47 °C.

Within further measurements a strong correlation of the temperature at the cell and its alternating switching off and on was detected. The time series of this measurement are presented in Fig. 11.The temperature increased until the PMT was switched off, then the temperature dropped slightly since the Peltier elements did not cool the PMT any more and therefore did not produce any waste heat. Once the temperature decreased approx. 0.2 °C, the PMT is switched on again leading to a rise in temperature and the peak in the O_3 signal. This cycle was then repeated.

When the instrument is operated without the top cover no complications arise during the measurement as the temperatures stabilise at approx 30 °C in contrast to 47 °C and the overheating does not occur.

Theses observations lead to the conclusion that the electronics of the PMT have a protective mechanism triggering the PMT power off at a threshold temperature, measured by an internal temperature sensor, in order to prevent overheating of the Peltier elements. This specific temperature is however hard to determine since the external temperature sensor measures the temperature at a different position as the internal temperature sensor of the PMT. This problem also gets evident from the fact that the temperatures at which this problem occurs are not constant and vary from measurement to measurement.

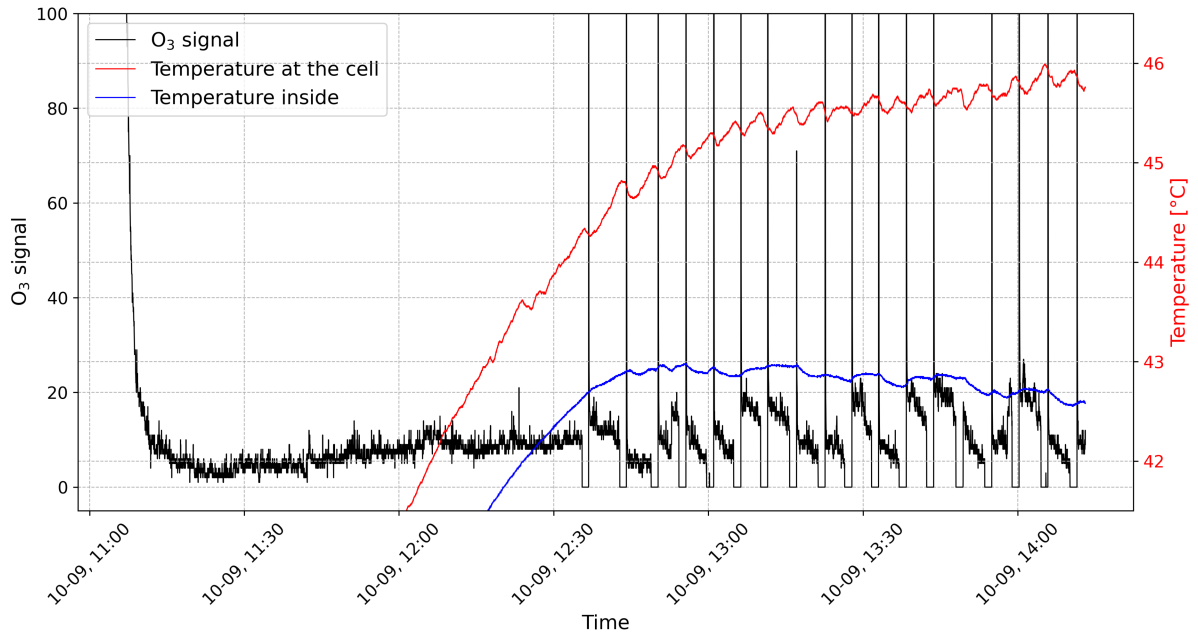

Figure 11: Zoom of the O_3 signal (*left axis*, black) and the temperatures (*right axis*, red) at the measurement cell (red) and inside the monitor (blue). The peaks in the O_3 signal correlate with the fluctuations in the temperature at the cell.

date	power supply	T_{start} [°C]	T_{stop} [°C]	time [min]	remark
27.08	power adaptor	29.2	42.7	86	
09.09	power adaptor	34.1	43.7	60	
10.09	power adaptor	34.5	44.5	22	
11.09	power adaptor	34.9	44.5	89	different power adaptor
11.09	power bank	42.5	47.4	80	directly after previous measurement
14.09	power adaptor	22.4	44.0	125	not additionally connected to ground
14.09	power adaptor	33.1	45.4	62	no CO2 sensor
16.09	power bank	21.6	47.0	257	several power banks enabling longer measurement time
17.09	mixed				
	power adaptor	21.0	44.62	190	switch in the power supply
	power bank	45.1	46.4	250	to power banks after overheating occurred with power adaptor

Table 6: Measurements during which the overheating of the monitor occurred. The method of power supply, the start temperature at the cell, T_{start}, and the temperature at the cell of the first power off, T_{stop}, as well as the time since power on when the first power off of the PMT occurred are listed alongside additional information.

In Tab. 6 the temperature and the time at which the overheating occurs are listed alongside the method of power supply. Additionally, the start temperature is listed in order to properly evaluate and compare the time after power on until the overheating occurs. It can be seen that higher temperatures are reached when the power bank is used and the measurement time at which the overheating occurs is considerably larger.

To counteract the overheating of the PMT a fan was installed. It is directed at the housing of the PMT to ensure better circulation and heat distribution inside the instrument leading to a longer operation time before the overheating. After the fan was installed in the CL monitor the overheating did not occur any more. The temperature at the cell stabilised at $\sim 42\,^{\circ}\mathrm{C}$ preventing the PMT power off due to overheating. The fact that this measurement was carried out during the winter, where considerably lower ambient temperatures are present as compared to summer, might have influenced this result.

5.1.5 Orientation dependence of the signal

We further observed that the signal increased when the monitor was placed upright (long side of the monitor is vertical, front panel faces upward), instead of its usual horizontal position (where the front panel faces forward). The quantification of this effect is of importance since the monitor's orientation is changed while it is moved, which is of particular importance during field measurements including movements. To quantify this effect the instrument was placed upright during calibration.

If zero gas from the O_3 generator was passed through the monitor no significant change in signal was visible upon changing the monitors orientation.
However, for higher O_3 mixing ratios (i.e. 150 ppb) a significant increase in the signal could be observed when the monitor was placed upright. Further experiments with higher O_3 mixing ratios (i.e. >150 ppb) were conducted. These measurements indicate that the rise in signal is proportional to the mixing ratio of O_3, the higher the O_3 mixing ratio the higher the rise in signal upon changing the monitors position.

Two of these calibrations are shown in Fig. 12, as examples. All values of the calibrations, are listed in Tab. 7, including the values for the respective O_3 mixing ratio for different positioning of the monitor, the absolute increase to the horizontal value, as well as the relative increase (in %). The relative increase is obtained with the following formula,

$$\text{relative increase} = \frac{\text{absolute increase}}{v_{150} - v_0}. \tag{54}$$

Even if the absolute rise in signal increases for higher O_3 mixing ratios, the relative increase tends to show a smaller value for higher O_3 mixing ratios when comparing the values for 150 ppb and the higher O_3 value.
Not only does the signal change when the monitor is placed upright but also if it is placed on its side. The corresponding values for each side are listed in Tab. 8. It can be seen that the signal increase is the largest when the monitor is placed upright, followed by positioning it on its right side. Smaller values (still higher than in the horizontal position) are obtained when the instrument is turned such that the front panel faces downward or the instrument lies on its left side.

It should be noted that the temperatures at the measurement cell and inside the monitor slightly drop (see Fig. 12), and the humidity increases if the instrument is placed upright.

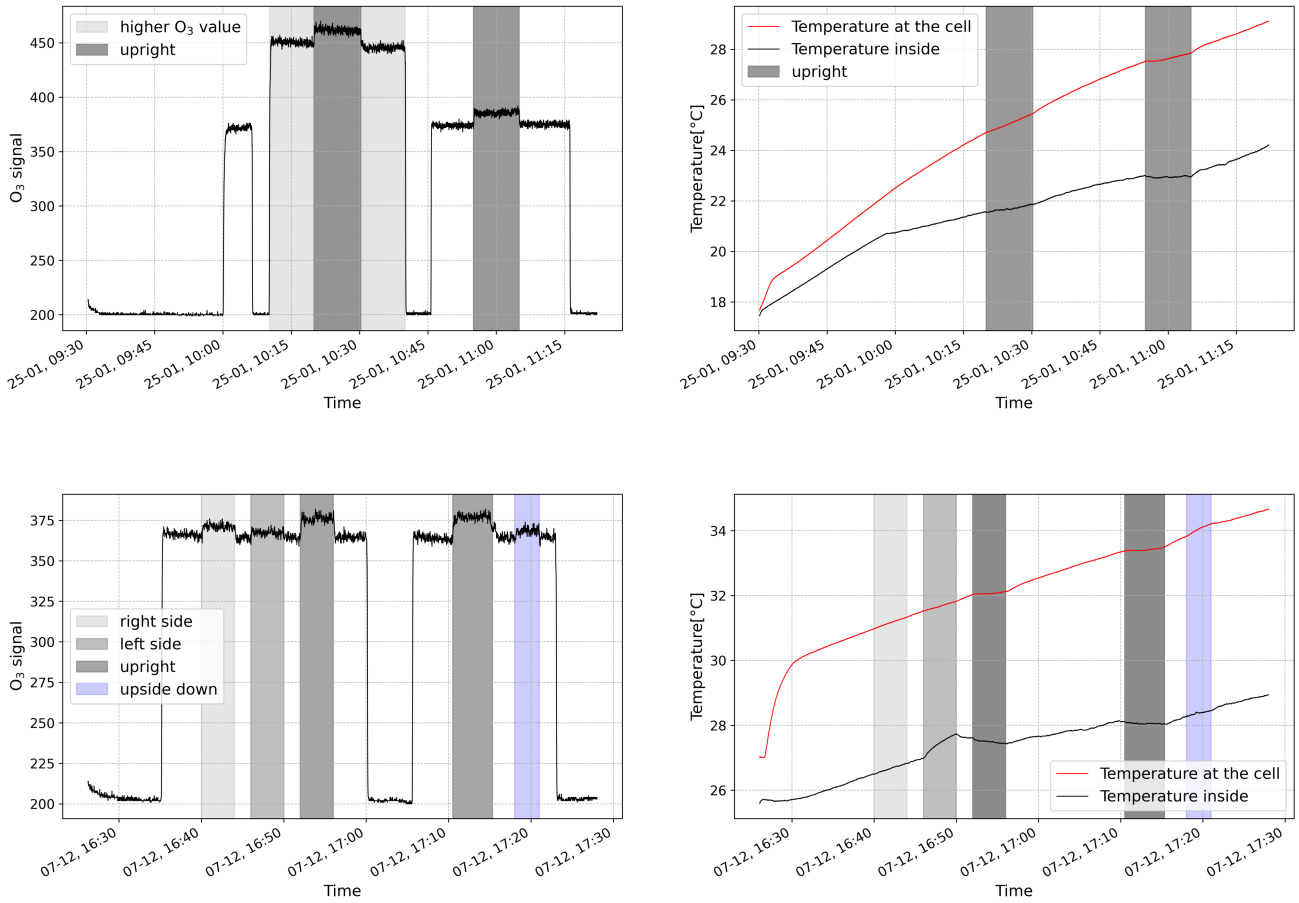

Figure 12: Calibrations during which the monitor's orientation was changed. Here, the O_3 signal (*left column*), the temperatures (*right column*) inside the monitor (black) and at the cell (red) are shown. An increase in signal can be seen for 150 ppb O_3, the increase is even larger for higher O_3 mixing ratios (*top*). It can be seen that the temperature slightly drops when the monitor is placed upright.
The rise in signal can also be observed if the monitor is placed on its other sides (*bottom*).

The change in the temperature inside the monitor might be explained by a change in air stratification within the instrument. However, the increase in signal can be unlikely attributed to these temperature variations since the change in temperature at the cell is even smaller and therefore a change inside the cell is even less probable. Furthermore, even if a temperature drop in the cell of roughly 0.5 °C is assumed the signal increase of approx. 7% can not be explained. On the contrary, for a decrease in the temperature also a decrease in the signal should be expected according to the calculations in Sec. 4.1.2.

Another attempt for an explanation is a change in the flow rate of the monitor when its position is changed. The flow rate through the measurement cell can be read off from a rotameter at the front panel. The basic functioning of the rotameter relies on a float inside a tapered tube, which is pushed up by the drag force and pulled down by the gravitational force. The drag force increases if the volumetric flow rate through a given area increases. As the area in the tube increases due to its tapered form the drag force decreases and a mechanical equilibrium between the drag force and the gravitational force on the float is established.

date	$v_{0\,\mathrm{ppb}}$ horizontal	$v_{150\,\mathrm{ppb}}$ horizontal	upright	deviation	higher O_3 value horizontal	upright	deviation
05.11	200.9 ± 0.7	365.6 ± 1.7	376.7 ± 1.5	13.3 (8 %)	-	-	-
13.11	200.1 ± 0.6	359.2 ± 1.5	371.9 ± 1.7	12.3 (7.7 %)	-	-	-
04.12	201.8 ± 0.4	358.5 ± 1.5	369.6 ± 1.5	11.3 (7 %)	-	-	-
07.12	201.9 ± 0.6	362.8 ± 1.7	374.3 ± 1.6	11.5 (7.1%)	-	-	-
07.12	202.3 ± 0.5	364.7 ± 1.7	376.6 ± 1.8	11.9 (7.4 %)	-	-	-
22.01	205.4 ± 1.4	371.9 ± 1.4	383.7 ± 2.1	11.8 (7.1%)	433.7 ± 2.1	449.3 ± 2.3	15.6 (6.8%)
25.01	200.5 ± 0.5	374.4 ± 1.2	385.6 ± 1.9	11.2 (6.4%)	448.0 ± 1.5	461.5 ± 2.3	13.5 (5.4%)

Table 7: Results for the calibrations during which the monitor's orientation was changed. All values for 0 ppb, 150 ppb and the higher O_3 mixing ratio for horizontally and vertically oriented monitor are listed. The total increase to the horizontal value and the relative increase (calculated as shown in Eqn. 54) are given.

date	horizontal	right side	deviation	left side	deviation	upside down	deviation
04.12	358.5 ± 1.8	364.2 ± 1.6	5.6 (3.6 %)	360.9 ± 1.6	2.5 (1.6 %)	-	-
07.12	365.1 ± 1.8	370.1 ± 1.8	5.1 (3.1 %)	368.5 ± 1.9	3.4 (2 %)	-	-
07.12	364.7 ± 1.7	371.2 ± 1.7	6.5 (4 %)	367.4 ± 1.6	2.7 (1.6 %)	368.6 ± 1.9	3.9 (1.6 %)

Table 8: Results for the calibrations during which the monitor was placed upright. All values for 0 ppb and 150 ppb of O_3 for horizontally and vertically oriented monitor are listed. The total increase to the horizontal value and the relative increases (calculated as shown in Eqn. 54) are given as well.

This means, as a corollary, that the pump inside the monitor has to work against the gravitational force acting on the float and therefore a different flow is expected when a rotameter is used compared to the flow when no rotameter is used.
If the instrument is placed upright the rotameter is oriented horizontally, instead of its usual vertical position so the gravitational force on the float does not counteract the drag force any more. This should result in a higher flow rate and might explain the increase of the signal when positioning the monitor in an upright position.

In order to test this assumption, the rotameter was removed. If a change in flow is caused by the positioning of the rotameter no such increase is expected upon changing the monitors position once it is removed. The values of the calibrations without rotameter are listed in Tab. 7, starting from the calibration carried out on the 4th December 2020. These do not show any deviation from the experiments during which the rotameter was still used. This then leads to the conclusion that the rotameter does not have a significant effect on the flow rate of the instrument and therefore the change in signal can not be attributed to the position dependence of the rotameter.

Nevertheless, the change in signal might still be traced back to a change in flow rate which occurs when the instrument is positioned differently. Therefore, an electronic flow meter was used to measure the flow. A measurement when the monitor was in a horizontal position was carried out, which yielded the expected flow rate of roughly $8.5\,\mathrm{ml\,s^{-1}}$ ($0.515\,\mathrm{L\,min^{-1}}$). After the monitor was placed upright another measurement was taken, this measurement gave a flow of $8.83\,\mathrm{ml\,s^{-1}}$ ($0.530\,\mathrm{L\,min^{-1}}$), which corresponds to an increase in flow of approx. 3%. A rough calculation however suggests, that an increase in the flow of approx. 3% should lead to an increase in signal of approx. only 2% in signal

and therefore can not account fully for the observed increase in signal (relative increase approx. 7%).

Ideally, this orientation dependence should be corrected in measurements. However, as this phenomenon is not fully understood it is hard to determine the appropriate correction. Since experiments on the orientation dependence of the signal for ambient air (around 20 ppb of O_3) have not shown any increase in signal, this effect is neglected for the measurements in this thesis.

5.2 UV absorption ozone monitor

5.2.1 Calibration

In order to be able to properly compare measurements from both monitors, a calibration of the POM has to be done. For the calibration the O_3 generator is used. Two of these calibrations are exemplary shown in Fig. 13. For the calibrations the adaptive filters of the monitor were disabled (for more details on the adaptive filters see Sec. 5.2.2) and a time resolution of 2 s was used.

All calibrations show the same structure.
The measurement of zero gas was done after a short warm up phase of several minutes. During this warm up phase the displayed values show great variability with fluctuations of several tens of ppb and even large negative values. This behaviour is expected and also mentioned in the manual and therefore the beginning of each measurement discarded.

Then, zero gas from the O_3 generator was passed through the monitor. Here the monitor displayed a value slightly below zero.
After the measurement of the zero gas the 150 ppb setting of the O_3 generator was used in order to quantify the reaction of the POM. The values measured by the POM greatly overshot the expected value of 150 ppb. After this initial overshoot, the signal decreased and approached the actual value for 150 ppb of O_3. However, the overshoot as well as the value obtained for 150 ppb was very variable.

There is also a slight undershoot when switching from 150 ppb to 0 ppb of O_3, visible for the two calibrations. It should be noted however, that this one is considerably less pronounced than the overshoot and is also almost instantaneously corrected as there is no slow convergence towards the zero value but rather a quick jump after the undershoot.

Since the values for the calibrations differ significantly, they are listed in Tab. 9 for comparison. Here, the values for 0 ppb, 150 ppb, the maximum value and time constant for the decrease after the initial overshoot are shown. For the value of 0 ppb the average over the timespan during which the zero gas was measured is calculated. The values for 150 ppb, the maximum value and time constant are obtained by fitting an exponential function to the data (see Eqn. 53). The value for 150 ppb is then given by the fit parameter c, the maximum value by $a + d$ and the time constant is equivalent to the fit parameter b.

The cause of the deviations between the calibration remains unclear.

date	value 0 ppb	value 150 ppb	max. value	time constant [min]	half time [min]
24.09	-1.5 ± 0.2	134.7 ± 0.1	290	3.10 ± 0.02	2.15 ± 0.01
		134.33 ± 0.04	171	2.19 ± 0.01	1.52 ± 0.01
28.09	-1.3 ± 1.0	125.8 ± 0.9	189	4.4 ± 0.4	3.1 ± 0.2
14.10	0.2 ± 1.1	194.5 ± 0.6	593	1.91 ± 0.01	1.3 ± 0.1
		170.3 ± 0.3	306	1.75 ± 0.02	1.21 ± 0.1
11.12	-0.9 ± 1.5	171.3 ± 0.8	1100	2.52 ± 0.02	1.75 ± 0.02
		153.2 ± 0.6	233	1.4 ± 0.1	0.98 ± 0.07

Table 9: Values for the calibrations of the POM. The corresponding plots are shown in Fig. 13. The values for 0 ppb are obtained by averaging over all periods during which zero gas from the O_3 generator was measured. The values for 150 ppb O_3, the maximum value and time constants are given by the fit parameters of an exponential function which was fitted to the data.

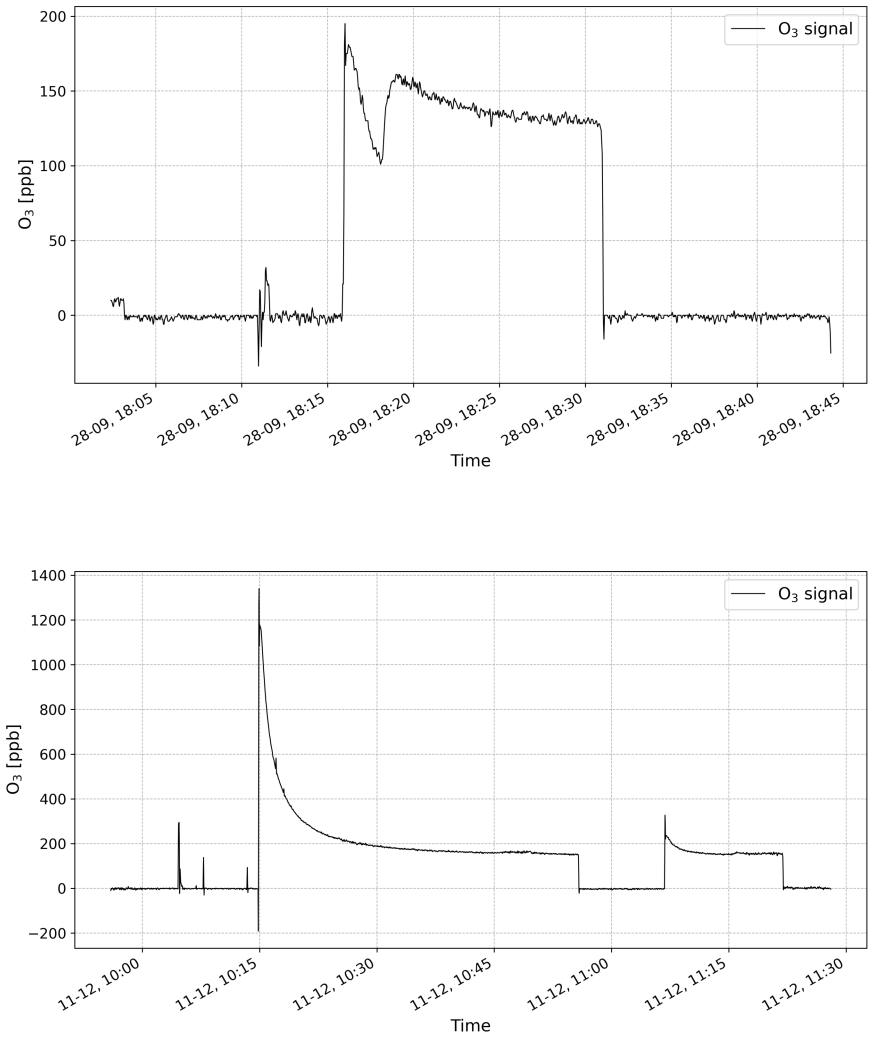

Figure 13: Calibrations of the POM. They exhibit large differences in the obtained values, the overall structure is, however, similar. A step change in the O_3 mixing ratios is accompanied by an over-/undershoot.

5.2.2 Measurements

Measurements of ambient O_3 have been carried out with the POM. One measurement can be seen in Fig. 14. In this measurement the ambient mixing ratios of O_3 inside the laboratory were recorded. During the measurement the window is opened and an increase in signal can be seen. This is expected since outdoor mixing ratios of O_3 exceed those inside due to the lack of O_3 sources inside and the gradual degradation of O_3. Therefore, after closing the window a slow decrease in the signal is expected, which can bee seen in Fig. 14. During this decrease a scrubber is fixed to the air inlet of the instrument. The signal needs several minutes to adapt to the change in O_3 mixing ratios. This relatively long reaction time to rapid changes in O_3 can be explained by the use of adaptive filters in the monitor. These adaptive data filters enable averaging over a certain number of measurement points in order to 'provide smooth and stable readings' when a relatively stable O_3 concentration is measured (POM, 2020). Only when rapid changes in the O_3 concentration (characterised by specific absolute and relative changes) are detected, the filter length changes to provide faster response times. More information on this can be found in the manual.
To enable faster response times in the adaptive filters were disabled all following measurements.

Another measurement was done to investigate the effects of shaking and moving the instrument, which is presented in Fig. 15. Times during which the instrument was moved, turned or shook lightly can be distinguished easily as they exhibit strong peaks in the O_3 signal. This has to be taken into account when interpreting the data.

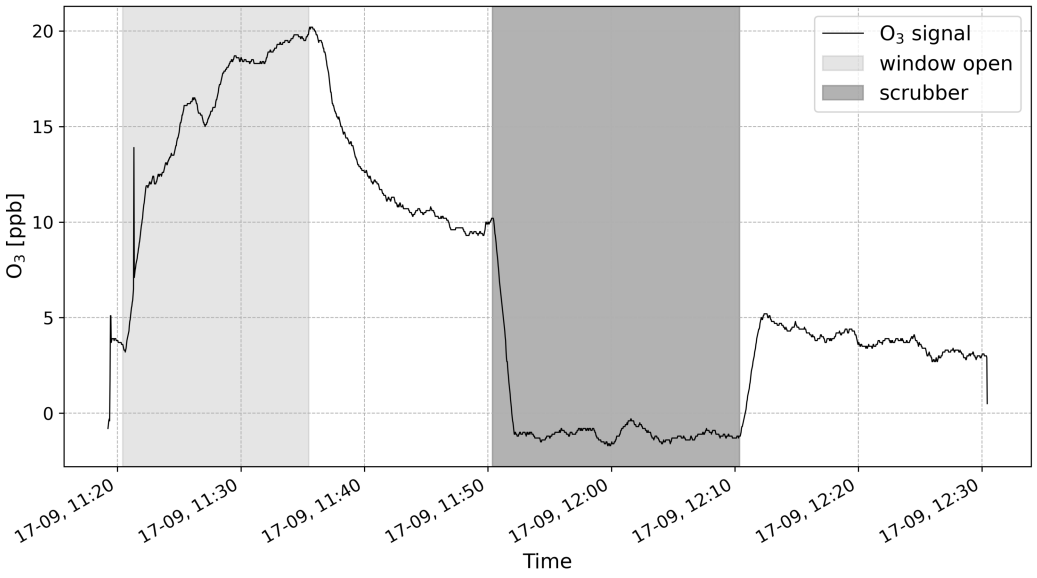

Figure 14: Measurement of ambient O_3 inside the laboratory with the UV absorption monitor. During the measurement the window was opened (highlighted light grey) leading to a flux of O_3 into the room. After closing the window the signal decreases. From 11:50 until 12:10 a scrubber was used (highlighted dark grey).

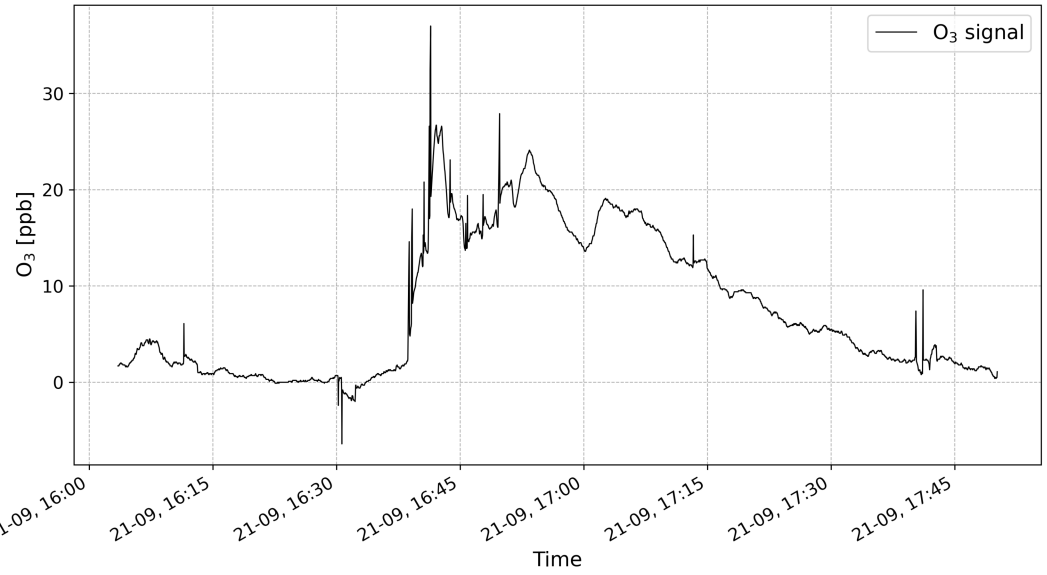

Figure 15: Measurement of ambient O_3 inside. During the measurement the monitor was shaken in order to quantify the monitors reaction to movement. Fluctuations, in particular peaks, associated with the shaking motion can bee seen. During the measurement the window was opened leading to the increase in signal.

6 Signal from 'glowing of ambient air'

While studying the dark current and its temperature dependence, an increase in the signal was observed when the window was opened even though no C_2H_4 was used. The effect is well above the detection limit and, at this moment, we can only explain it by assuming luminescent processes (similar to the reaction of O_3 with C_2H_4) in the ambient air.

When studying the dark current of the PMT no photons should enter it and therefore, in this case, no chemiluminescent chemical reaction should proceed in the measurement cell. In order to prevent this the absence of either one or both of the reactants needs to be ensured. This can be done by not opening the C_2H_4 minican, using a scrubber, using zero gas from the O_3 generator or a combinations of the three. The measured signal of either one of these configurations should equal the dark current of the PMT as no chemiluminescent reactions of O_3 with C_2H_4 can take place.

If only ambient air without the injection of C_2H_4 is passed trough the instrument and the laboratory window is closed, this configuration indeed enables the measurement of the dark current. This can be established since there is no drop in signal when a scrubber is attached to the air inlet so the obtained value equals the zero value (values obtained without C_2H_4 and with a scrubber or zero gas from the O_3 generator). However, an increase in the signal could be observed when no scrubber was used the window was opened allowing outside air to enter the room. The signal exceeds the zero value by a few ppb which then leads to a distinct drop in signal when attaching a scrubber to the air inlet. After closing the window a slow decrease in the signal can be observed and the signal approaches again the zero value. In Fig. 16 one of these measurements is shown. Due to the characteristics of the signal when a scrubber is used, the hypothesis is supported that it arises from fluorescent/phosphorescent components in the air rather than from photons entering the measurement cell trough gaps. This apparently 'glowing air' might be induced by chemical reactions with excited species as products, which emit photons on their de-excitation. Two scenarios may explain the observed signal:

1. The reaction, $O_3 + Y \longrightarrow$ products,
   is responsible for the signal. This is not far-fetched as reactions with O_3 are know to often produce CL. This scenario would not disturb ambient O_3 measurements since if C_2H_4 is available in excess (compared to Y) almost all O_3 molecules would react with C_2H_4.
2. The reaction, $X + Y \longrightarrow$ products,
   causes the signal. If this is the case, also during O_3 measurements with C_2H_4 the signal from this reaction would consequently be measured acting as a non-constant offset. This entails that ambient O_3 measurements with a CL monitor are not as precise as previously thought.

To obtain indications on the origin of the measured signal one measurement was made during the day and one in the evening without sunlight. These measurements do not show significant differences. For both measurements an increase of ~ 4 ppb equivalent O_3 signal was registered. Since the signal is still visible with the same strength when there is no sunlight the cause for this signal is presumably not closely related to photo chemical reactions in the atmosphere.

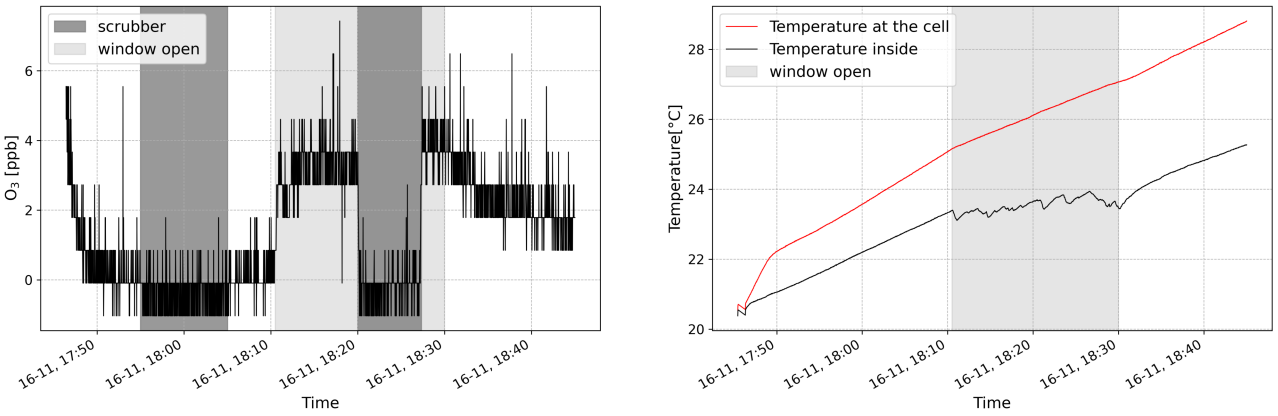

Figure 16: Measurement of the 'glowing air'. The time series of O_3 (*left*) and the temperatures (*right*) inside the monitor (black) and at the measurement cell (red) are shown. Periods during which a scrubber was used and during which the window was open, which can be clearly distinguished in the temperature, are marked. An increase in the O_3 signal can be observed as soon the window is opened. If a scrubber is attached to the air inlet the O_3 signal drops.

It has to be noted that the strength of the increase in signal is not always constant. In particular, during one measurement the rise in signal when the window was opened was noticeably reduced with an increase of only 2 ppb. This measurement was done in the afternoon and it was considerably cloudier than during the measurements shown in Fig. 16. However, if the change in cloudiness is the cause for the deviation between the measurements yet remains unclear.

To further investigate the cause of the signal, parallel O_3 measurements with the POM were carried out. One of these measurements is shown in Fig. 17, where the signals of both monitors are shown as an overlay to better compare them. The time during which a scrubber was used or when the window was open are marked. This experiment was carried out in winter during fair weather, only few clouds at roughly 10 °C. During this measurement the glowing of the ambient air was one of the strongest observed, with the signal reaching ~ 10 ppb equivalent O_3.
After closing the window the gradual decrease in both signals can be observed. The time constant and the half-life of the decrease are obtained by fitting exponential functions to the data (see Eqn. 53). The half-life is then obtained from the time constant b of the exponential function by

$$T_{1/2} = \ln(2) \cdot b. \tag{55}$$

This approach yields a half-life of $T_{1/2} = 21$ min and $T_{1/2} = 15$ min for the first and the second decrease observed in the signal, respectively. Additionally, exponential functions were fitted to the decrease in the O_3 signal of the UV absorption monitor. For the first and second decrease the half times $T_{1/2} = 31$ min and $T_{1/2} = 21$ min were obtained.

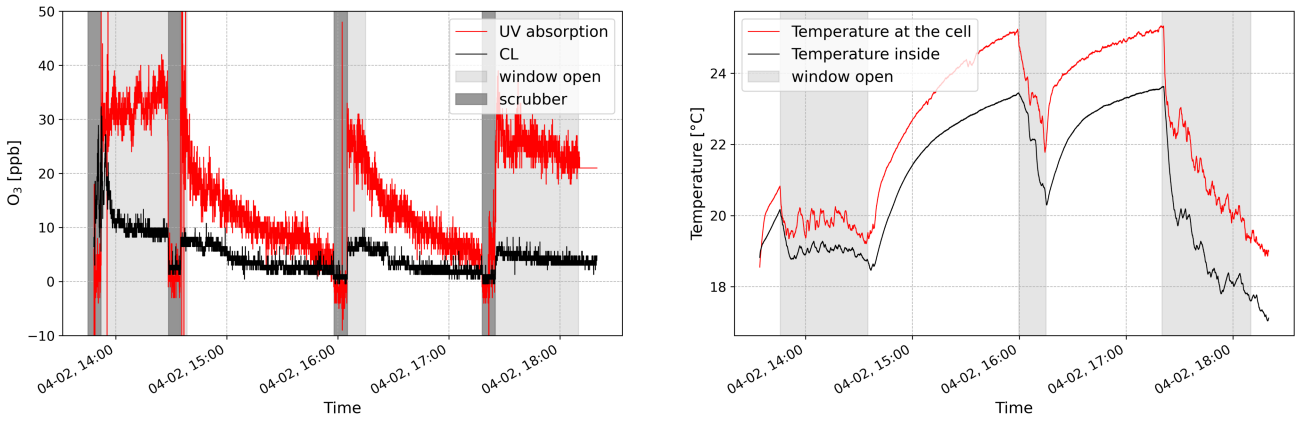

Figure 17: Measurment of the 'glowing air'. In parallel O_3 measurements with the POM were made. The O_3 signals (*left*) from the CL monitor (black) and the UV absorption monitor (red), as well as the temperatures (*right*) inside the monitor (black) and at the measurement cell (red) are shown. Periods during which a scrubber was used are indicated by dark grey shading, an open window is marked by light grey shading.

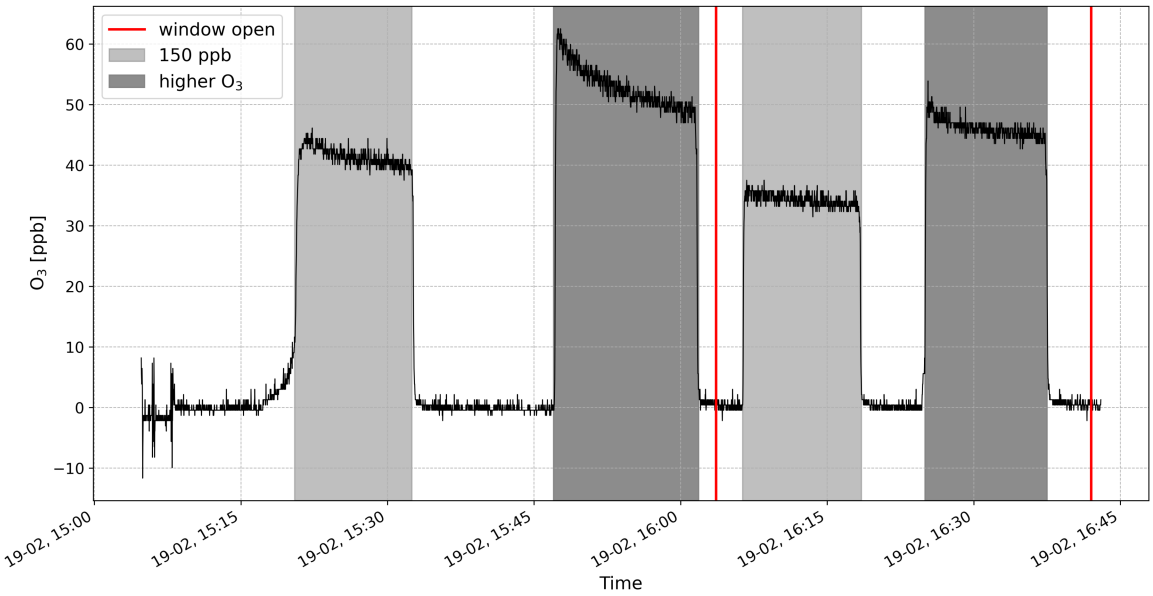

Figure 18: Measurement with the CL monitor without the injection of C_2H_4. The O_3 generator is used to provide 150 ppb (highlighted in light grey) and a higher mixing ratios of O_3 (highlighted in dark grey, $\approx$ 250 ppb). The experiment was carried out once with the window closed and with the window open (period between two red lines).

Additionally, gas from the O_3 generator had been measured without the injection of C_2H_4. In particular, air containing 150 ppb as well as a higher O_3 mixing ratios have been used and the experiment has been carried out once with the window closed and once with the window opened. The results are presented in Fig. 18. When the window is closed, the signal does displays higher values compared to when the window is open. The signal takes on values of 41.5±1.5 ppb and 52.8±3.3 ppb for 150 ppb O_3 and the higher O_3 mixing ratio of around 250 ppb, respectively, if the window is closed. When the window is opened, values of 34.3±1.0 ppb and 46.1±1.4 ppb are measured for 150 ppb O_3 and the higher O_3 mixing ratio, respectively. However, in particular for the higher O_3 mixing ratio the signal clearly decreases during the course of the measurement. This decrease in signal even when constant mixing ratios of O_3 were measured has been seen in other calibrations before so the deviations between the first part of the measurement during which the window was closed and the second part during which the the window was open can probably not be attributed to opening or closing the window.
It is still not clear whether the observed signal from the O_3 generator is related to the signal which is observed when the window is opened. The O_3 generator could produce additional species which might cause a chemiluminescent reaction.

7 Comparative ambient measurements

7.1 Experimental setup and methods

In order to compare both instruments it is important that the same conditions are prevalent in both measurements. This means that the same air is sampled at the same time in both monitors.
In particular, the timing relationship between the two signals is crucial. There are several approaches to reliably determine this relationship.
The most straightforward approach is arguably the synchronisation of the internal clocks of the instruments with respect to each other. However, a precise timing of both clocks was not possible. For the CL O_3 monitor the clock can be set by uploading code to the Arduino, as soon as the code is uploaded the time is set. This is unavoidably linked to inaccuracies when setting the time. Additionally, drift of the clock is common and also observed in this instrument accounting for several seconds a day.
The internal clock of the POM can be set in the menu accessible via the front panel. Here, the time has to be entered in advance as well and is then set when the menu is left. This process is also afflicted with the uncertainty of when the time is set exactly and therefore impedes a precise setting of the time.
Since the above method is rather error prone, the approach of cross correlation is used, where distinct and well defined events visible in both signals allow for time synchronisation (e.g. simultaneous step changes in the O_3 mixing ratios). During the measurements scrubbers were removed or fixed to the air inlets of both instruments simultaneously. The resulting step changes in the O_3 mixing ratios then allowed for synchronisation of the signals of both the CL monitor and the UV absorption monitor. This procedure was applied to all measurements.
Upon removing the scrubbers, tubes were fixed to the air inlets to supply the instruments with ambient air. The tubes were tied together at the other end to ensure sampling of the same air.

The signal of the CL monitor is calibrated using the calibration performed before the respective measurement. Additionally, further zero-point corrections might be done by averaging over the time periods during which a scrubber was used and subtracting this value instead of the value obtained in the calibration.
The only data processing that was done to the signal from the POM is a zero-point adjustment.

7.2 Results

In Fig. 19 measurements of ambient O_3 with both monitors are shown. In the upper part, the time series of both signals is shown as an overlay, in the lower part, the two signals are plotted against each other. For both signals a zero-point adjustment has been carried out.

The two monitors display similar trends in the time series of O_3 which deviate from each other only for small periods (e.g. shortly after the scrubber has been removed for the second time). In the beginning of the measurement the UV absorption monitor displays peaks in the signal which can with high probability be traced back to 'shaking' the instrument. Here, the scrubber was removed and the tube was fixed to the air inlet

which led to some minor vibrations of the instrument. To circumvent further disturbances of the signal, the scrubbers were then fixed to the end of the tubes (for both instruments) so that the POM did not experience any further movements.

The scatter plot in the lower part of Fig. 19 indicates a good linear correlation of the signals. Their correlation is determined by a linear fit, which exhibits a slope slightly exceeding one and a small positive intercept. For the fit an R^2 value of 0.72 is obtained. In the time series one can see, that the UV absorption monitor does display slightly higher O_3 values which probably causes the slope of the linear function to slightly exceed one.

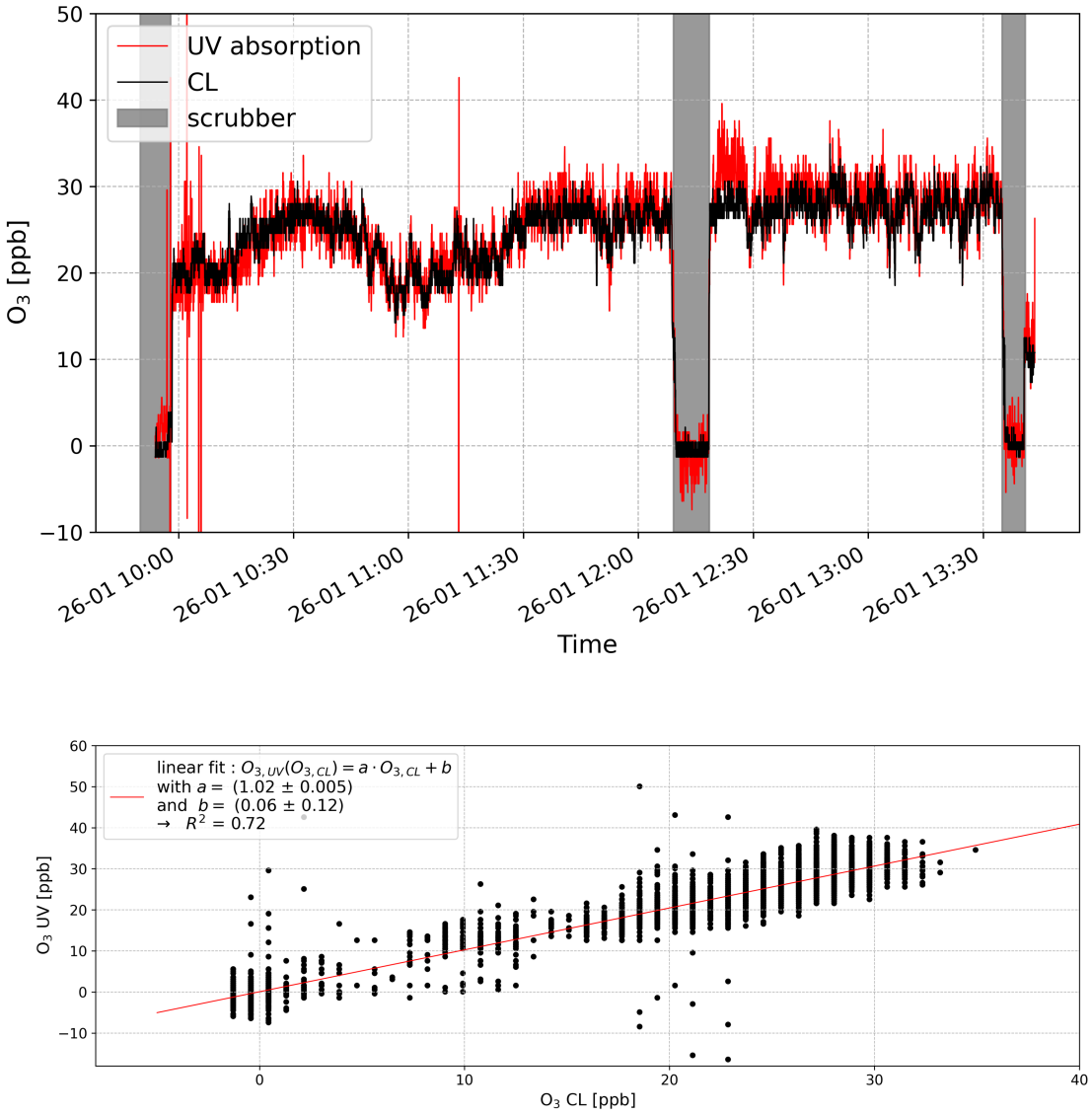

Figure 19: Direct comparison of the time series O_3 signal (*top*) of the CL (black) and UV absorption monitor (red). The CL signal is calibrated with a previously performed calibration, the UV signal is not processed except a zero-point adjustment. Additionally, both signals are plotted against each other and their correlation is determined using a linear fit (*bottom*). The fit with its fit parameters and the R^2 value is shown.

8 Field measurements at Mt. Etna

8.1 Location

Etna is located at the eastern coastline of Sicily and is known to be one of the largest and most active continental volcanoes worldwide (Bobrowski and Platt, 2007; Bobrowski et al., 2007). Etna has undergone eruptive as well as quiescent periods with eruptions being documented since the Greek colonisation (700 BC). Its activity, however, dates back further, starting about 0.6 Ma ago (Branca et al., 2004).

Structural and morphologic changes have formed the summit area of the volcano. Especially the evolution in twentieth century, shaped the current structure of the summit area. Today, Etna has four active summit craters, namely Bocca Nuova (BN, 1968), Voragine (VOR, 1968), Southeast (SEC,1978) and Northeast crater (NEC, 1911) (Branca and Del Carlo, 2004).

At the time of the measurements, Etnas activity was dominated by strombolian eruptions by the SEC and NEC and sporadic explosions of ash by the VOR. Therefore an in-situ measurement of the strong plume emitted by the SEC was not possible as the conditions were too hazardous. The other craters unfortunately did not emit strong defined plumes desirable for in-situ measurements.

Since no plume measurements were possible at the time of the field campaign measurements were conducted inside a fumarolic plume. However, fumarolic emissions are much weaker in comparison with the main crater plumes and show higher air contamination. Important factors strongly influencing the gas composition of a fumarole are e.g. its temperature. Inside the plume of a fumarole no local O_3 depletion is expected due to the low amount of reactive halogen species emitted. Nevertheless, as high mixing ratios of SO_2 and other species of volcanic trace gases are common inside the plumes of fumaroles the response of the CL and UV absorption monitor to high mixing ratios of volcanic trace gases can be studied and compared.

The measurement shown here was done on the 2nd October 2020 inside a fumarolic plume at the south eastern flank of the BN (N37°45.007′, E14°59.472′; altitude: 3303 m).
During the measurement it was sunny, with smaller clouds at a temperature of approx. 8 °C. The wind came mainly from the west.

8.2 Instrumentation and methods

For the measurements at Mt. Etna the following instruments were used:

- CL O_3 monitor
- UV absorption O_3 monitor → POM
- SO_2/CO_2 gas sensor → Sunkist

The CL O_3 monitor and the POM have been described and characterised previously in Sec. 4 and 5.
The Sunkist is a multi-gas instrument measuring CO_2 and SO_2 simultaneously. The operation principle of the CO_2 sensor relies on the measurement of the attenuation of near infrared light along a well defined path (analogous to the UV absorption O_3 monitor).
To measure SO_2 a electrochemical sensor is used, where a compensating current is mea-

sured which is caused by oxidation of SO_2 on one of the sensors electrodes (Rüdiger et al., 2018).

As mentioned in the previously (see Sec. 7), when using several instruments during a measurement it is important to establish their timing relation. The method to determine the timing relationship between the two O_3 monitors is explained in detail in Sec. 7.
A similar approach was taken to synchronize the measurement data from the Sunkist with the O_3 monitors. Here, the multi-gas instrument was switched on when the warm up phase of the CL monitor was over and the C_2H_4 minican was opened resulting in a step increase in the signal of the CL monitor.

In order to obtain the mixing ratios of O_3 from the signal of the CL monitor the calibration procedure explained in Sec. 5.1.1 is used. Here, the values of the calibration performed before the field measurement, on the 30th September 2020, were used.
Analogous to the calibration of the CL monitor, usually a calibration of the Sunkist is used to obtain the mixing ratios of SO_2 and CO_2. Unfortunately, this calibration has not been performed until now due to technical issues.
Usually, no processing of the UV absorption data is needed. However, UV absorption monitors show significant interference with SO_2 as discussed in Sec. 4.2.2. To correct the measured O_3 values for SO_2 interferences the measured O_3 data is plotted against the measured SO_2 mixing ratios. From this the relation of O_3 and SO_2 values can be obtained by applying a linear fit to the data,

$$[O_3] = a_{SO_2} \cdot [SO_2] + b. \tag{56}$$

The fit parameter a_{SO_2} can then be used as a correction factor for O_3 measurements and with the following relation the O_3 mixing ratios can be corrected for SO_2 interferences

$$[O_3]_{corr} = [O_3]_{meas} - a_{SO_2} \cdot [SO_2]. \tag{57}$$

A better method would be to determine the response of the UV absorption monitor towards SO_2 in laboratory experiment using calibration gas.

8.3 Measurement results

In Fig. 20 the time series of the mixing ratios of O_3, SO_2 and CO_2 as well a pressure, temperature and humidity are shown. In the plot periods within the plume of the fumarole are marked. No O_3 depletion could be seen in the measurements of both O_3 monitors inside the fumarole.

In Fig. 21 *top* a direct comparison of the O_3 signals from both monitors and the SO_2 signal is shown. Here, no processing of the UV absorption data except a zero-point adjustment was done, the data of the CL monitor was modified as explained above.
For the parts of the measurement during which ambient air was measured, both O_3 monitors display similar trends in the time series. During this part comparatively little volcanic gases, in particular SO_2, were measured compared to the period inside the fumarole. Still, an offset of $\sim$20 ppb of the UV absorption signal compared to the signal from the CL instrument is visible which can probably traced back to SO_2 in ambient air.

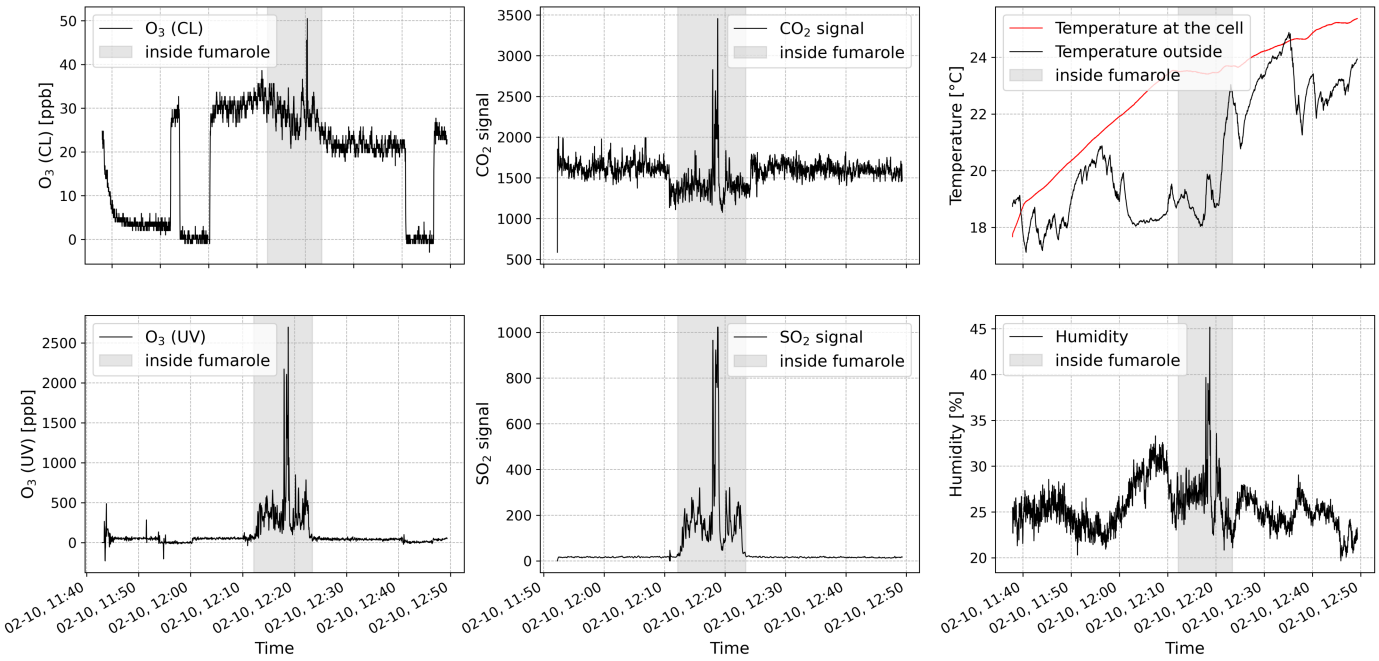

Figure 20: Time series of different parameters measured during the field campaign at the summit of Etna. The measurements of O_3 with the CL monitor (*top left*) and the UV absorption monitor(*bottom left*), CO_2 (*top centre*) and SO_2 (*bottom centre*) measurements with the Sunkist as well as the the time series of the temperature (*top right*) and humidity (*bottom right*) (measured with the CL monitor) are shown. The part inside the fumarolic plume are marked.

The part during which fumarolic emissions were measured can be distinguished easily in Fig. 21 as the signal of the UV absorption monitor displays significantly increased values of O_3 mixing ratios whereas the signal from the CL monitor stays relatively constant. It can be seen that the signals of the UV absorption monitor and the SO_2 signal from the Sunkist display very similar time series. As mentioned earlier, changes in the signal of the UV absorption instrument have to be expected not only due to high SO_2 mixing ratios but also due to the motion of the monitor. The fluctuations and peaks in the signal which can be observed before SO_2 mixing ratios increase are probably related to moving the instrument.
To better quantify the correlation of the two signals a scatter plot of the two datasets was made and is shown in the lower part of Fig. 21. A linear function was fitted to the data to obtain their correlation, the fit as well as the fit parameters are also shown in the plot. For the fit an R^2 value of 0.90 is obtained. This good correlation between the two signals implies that the main part of the increase in the signal of the UV absorption monitor can be attributed to positive interference from SO_2. Deviations from the linear dependence might be attributed to jumps in the O_3 signal which arise when the instrument is moved.

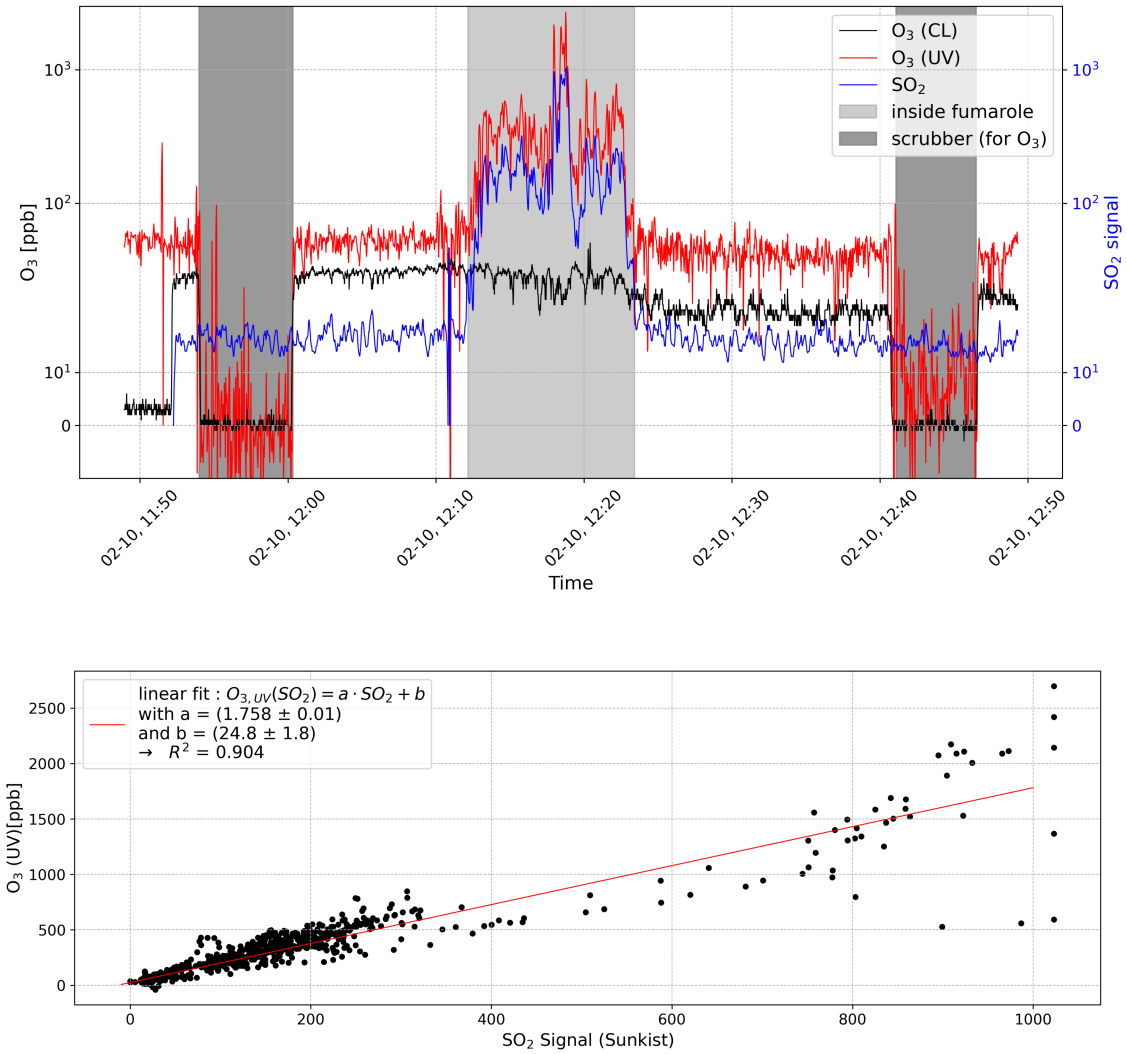

Figure 21: Direct comparison (*top*) of the O_3 signal of the CL (black), of the UV absorption monitor (red) and the SO_2 signal from the Sunkist (blue). The scatter plot of the O_3 signal from the UV absorption and the SO_2 signal (*bottom*) is sown. To determine the correlation of the two signal a linear function (red) is fitted to the data, its fit parameters and the R^2 value are listed in the plot.

With the slope a of the linear function the O_3 signal can be corrected, as explained in Sec. 8.2. The corrected values of the O_3 signal of the UV absorption monitor alongside the signal of the CL monitor are presented in Fig. 22.
The periods during which ambient air outside of the fumarolic plume was measured now display slightly lower values for the UV absorption monitor compared to the CL signal. The part of the measurement in the fumarole with increased SO_2 values is still characterised by tremendous deviations between the two signals. These discrepancies can also be clearly seen in the scatter plot in the lower part of Fig. 22 which is also reflected in the poor R^2 value of 0.028. In this case, even the corrected O_3 signal from the UV absorption monitor does not display reliable O_3 mixing ratios The deviations might be traced back to inaccuracy in time alignment of the SO_2 signal and the O_3 signal of the UV absorption monitor or to the above mentioned fluctuations in the signal induced by movements of the UV absorption monitor.

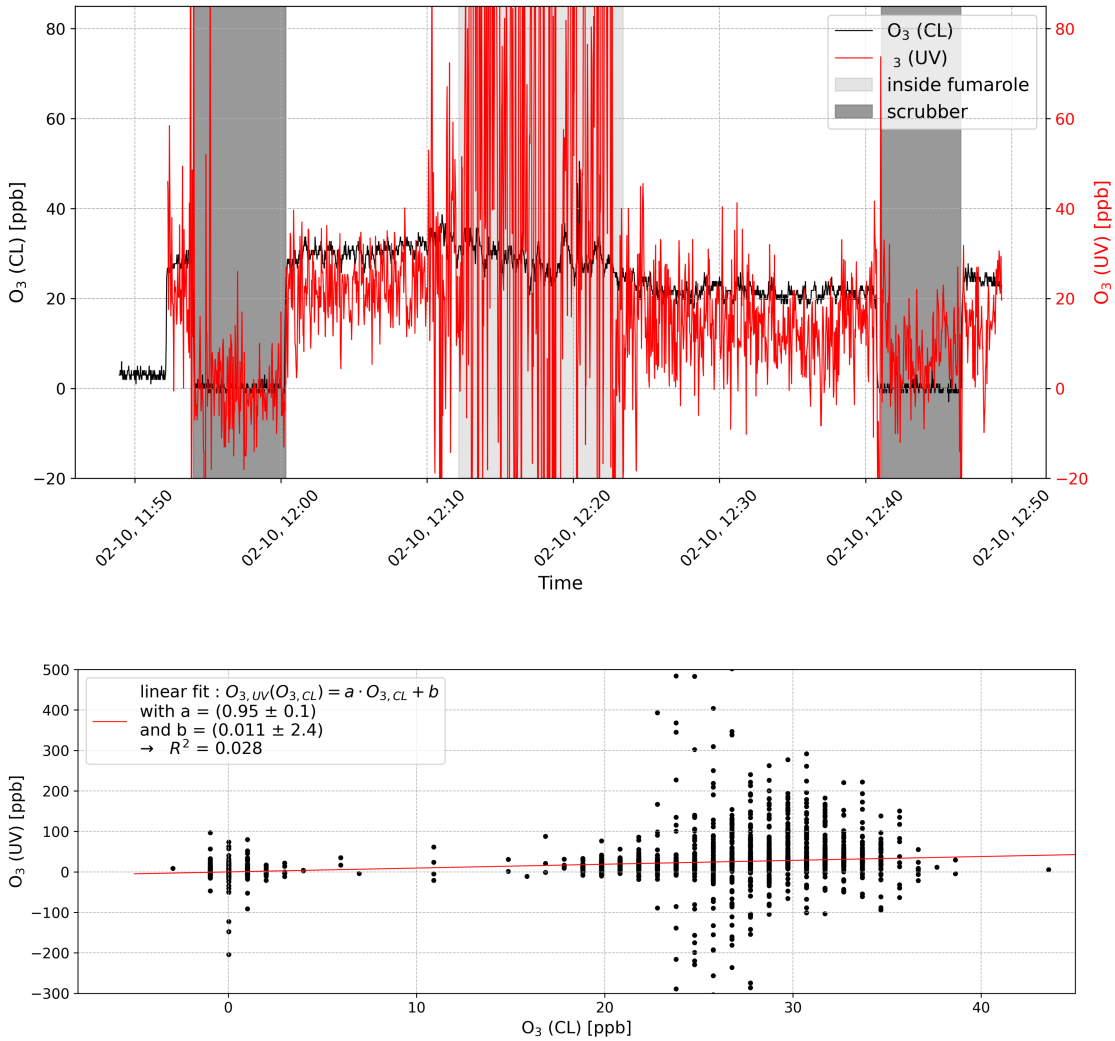

Figure 22: Direct comparison (*top*) of the O_3 signal of the CL (black) and the corrected signal of the UV absorption monitor (red). Additionally, the scatter plot (*bottom*) of the two signals with linear fit (red) to determine their correlation is shown. The fit parameters and the R^2 value are listed.

9 Discussion and outlook

In this thesis a CL O_3 monitor was characterised. The monitor has a detection limit of 1 ppb in laboratory experiments as well as under field conditions and reacts to step changes in O_3 mixing ratios with a time constant of ~ 2 s.
As the calibrations show a drift without adjusting the potentiometers for the 'zero value' and the 'span', with deviations of up to 15% from the originally measured values, the need for regular calibration becomes apparent. This is, however, only valid if the changes in the measured O_3 mixing ratios have their cause within the CL monitor itself. However, this drift in calibrations could also be attributed to the used O_3 generator producing unreliable mixing ratios of O_3. Strong deviations in the calibration of the UV absorption monitor were observed as well which strengthen the assumption of the O_3 generator to unreliably produce 150 ppb. But even the deviations in the UV absorption monitor can not with certainty be accounted for with changes in the O_3 generator.

Additionally, the signal of the CL monitor shows a dependence on the orientation of the monitor. The highest increase in signal can be observed when the monitor is placed upright (long side of the monitor is vertical, front panel faces upward), with relative increases of up to 8%, but also when the monitor lies on its right or left side an signal increase was seen, showing relative increases of up to 4% and 2%, respectively.
These changes in signal might be explained by a change in flow. In an upright position the flow is increased by approx. 3%. This increase in flow does, however, not suffice to explain the rise in signal fully as it should only account for an increase of $\sim 2\%$. In further experiments the cause of the orientation dependence of the signal should be studied and characterised as for future measurements a correction of this effect is desirable.

A study was carried out to determine the temperature dependence of the CL monitor's signal, which includes the temperature dependence of the dark current as well as of the reaction itself. No signifiant temperature dependence of the dark current is observed. When using power banks to power the instrument and for temperatures at the cell between 17 °C and 40 °C only a slight increase in the signal of below 2 ppb is apparent. A slightly higher increase can be observed when the temperature exceeds 40 °C, with values of around 3 ppb. For the use of the external power adaptor higher increases of around 10 ppb occurred, which however can be considered as outliers. Still, when operating the monitor with the power adaptor this should be kept in mind.
The temperature dependence of the signal for an O_3 mixing ratio of 150 ppb generally exhibits values between 0.6 ppb $\cdot$ K^{-1} and 1.4 ppb $\cdot$ K^{-1}, however, during some periods the signal did not increase with temperature at all. To explain the differences in the temperature dependence changes in the ambient conditions, such as pressure or humidity, have been considered but no apparent relation was noticeable. Here again, changes in the mixing ratios in O_3 from the generator might be responsible for some part of the deviations. Also, the effect of quenching of the chemiluminescent species from the O_3-C_2H_4 reaction is still not clear and potentially influenced the obtained results for the temperature dependence.
Generally speaking, temperature of under 40 °C at the cell are desirable since the probability for the signal to show unexpected behaviour increases for temperatures exceeding 40 °C. The reason for this remains yet unclear.
For all field measurements shown here this posed no problem, as temperatures were always below 40 °C. Still, for further measurements this should be kept mind and should preferably be conducted in the shade to prevent overheating of the instrument.

In laboratory experiments it is preferable to not close the lid of the monitor, since it limits the temperature increase to about 30 °C. It is desirable to further characterise the temperature dependence of the signal to allow an accurate correction. To do this, it might be helpful to determine the temperature dependence of a signal for other O_3 mixing ratios than 150 ppb. In particular, values closer to ambient mixing ratios of O_3 could help to evaluate the importance of the temperature dependence.

Another interesting observation was a signal that occurred when ambient air without the addition of C_2H_4 was measured. This signal was unusual since it is expected that with the absence of one reactant needed for the chemiluminescent reaction no signal should be detected. An increase in signal starting from the zero value and reaching values of nearly 10 ppb equivalent O_3 signal was observed when the window was opened and it disappeared within approx. 1 h after the window was closed again or instantaneously when a scrubber was fixed to the air inlet. The decrease in signal showed the characteristics of an exponential decrease with a time constant between 15 min and 20 min. These observations lead to the conclusion that the signal does not arise from possible light leakage into the PMT but rather from chemiluminescent reactions taking place in the ambient air and in the measurement cell. This observed CL might be explained by reactions of an unknown substance with O_3 or by the reaction of two unknown substances. The latter would pose a significant problem as the observed signal would then act as a not constant offset during measurements.
The signal can also be observed when it is dark, so most probably it is not closely related to photochemical reactions. Parallel measurements of O_3 with the UV absorption monitor show similar trends in the time series compared to the signal of the 'glowing air' with the CL monitor. This observation does, however, not necessarily indicate that the unknown reaction causing the signal is a reaction involving O_3. It rather shows that one or both of the reactants might correlate with O_3. Also, measurements without the injection of C_2H_4 and with the O_3 generator show a signal. When the window is closed during the experiment higher values in the CL monitors signal can be observed compared to when the window is opened. However, these higher values, which also show a significant decrease during the course of the measurement, can be probably traced back to instabilities within the monitor rather than to the opening or closing the window (for some calibrations a similar effect was observed, where the signal decreases even though constant mixing ratios of O_3 were measured).
Overall, the cause of the observed signal from 'glowing air' yet remains unclear and more measurements are needed to characterise it further. A long-term measurement of the signal with a parallel O_3 measurement with the UV absorption monitor might provide further findings.

Additionally, the CL O_3 monitor was compared to an UV absorption O_3 monitor. During the calibration of the UV absorption monitor deviations were observed. Since the operation principle of the UV absorption monitor is an absolute one, so no calibrations should be needed, this might hint at changing O_3 mixing ratios produced with the generator (as mentioned above). Furthermore, the signal of the UV absorption monitor was found to exhibit peaks when moved or shook. This is however, not a characteristic of UV absorption monitors in general but rather of the specific model (POM) itself.

	advantages	disadvantages
CL	– no interference from trace gases	– need for reactant gas – less easily portable – orientation dependence of signal (can be corrected)
UV (POM)	– small, lightweight – little power consumption	– positive interference with SO_2 (hard to correct) – change in signal when moving (hard to correct) – overshoot for high step increases in O_3 concentration

Table 10: Advantages and disadvantages of the CL monitor characterised in this thesis and the POM, UV absorption monitor.

In Tab. 10 the advantages and disadvantages of each monitor are listed.
It is apparent that depending on the specific application different O_3 monitors should be chosen to obtain the most reliable measurements. For ambient O_3 measurements, as studies have already shown, no significant interference from trace gases in the signal from UV monitors is expected. This makes UV absorption monitors preferable over CL O_3 monitors in this field of application since they are more easily manageable due to the lack of reactant gas.

For volcanic applications the situation is different. The strong interference in the signal of the UV absorption monitor from SO_2 was clearly visible in our measurement inside the plume emanating from a fumarole. Even correcting the O_3 signal for SO_2 interference did not yield sensible values. This might, however, be partly traced back to the fluctuations in signal upon moving the UV absorption monitor. The CL monitor did not show any interference with volcanic gases. Therefore, even though the usage of the CL monitor might still entail inconveniences (relatively heavy and bulky instrument, need for reactant gas, higher power consumption) which are especially noticeable during field measurements, the advantage of reliable measurements within volcanic plumes strongly outweighs these inconveniences.

The demonstrated O_3 measurements based on the CL technique are a promising approach to provide reliable O_3 measurements in volcanic plumes. Still, further improvements of the monitor are needed to ease measurements inside volcanic plumes, in particular, the reduction of the monitors weight and size. This might be accomplished by replacing the heavy metal base on which the operation unit is fixed and using a modern PMT. This would then not only reduce weight as no heavy aluminium housing is needed but it would also enable to slim down the electronics needed for its operation. A reducing in size of the instrument is limited since a C_2H_4 minican has to be accommodated inside.
Additionally, it would be beneficial if the CL monitor would be equipped with an internal GPS sensor and a CO_2 sensor. Generally, the prerequisites for both modules are given. However, technical issues such as too little memory on the Arduino for the needed code have prevented their installation.
These smaller shortcomings could be rather easily solved in our case since stationary in-situ measurements were carried out, so the GPS coordinates as well as parallel CO_2 and SO_2 could be measured with other instruments. However, when the monitor is, as

originally intended, operated from a drone these alterations are necessary. This would enable to measure O_3 profiles in volcanic plumes which would provide insight into the distribution of O_3 inside the plume. These measurements might help to verify existing theories and clarify whether the assumption of bromine catalysed O_3 loss in volcanic plumes is valid.

This is of particular interest since our assessment calculations suggest that no local O_3 loss in volcanic plumes should be expected. We showed that O_3 inside the plume would be quickly replenished by mixing of ambient O_3 into the plume as the influx of O_3 exceeds the destruction by two orders of magnitude (see Sec. 3). Therefore the assumption of a local O_3 hole inside the volcanic plume was refuted for the plume geometry assumed here. This finally raises the question: "Is there an O_3 depletion within volcanic plumes?" and stresses the importance of further and more reliable measurements.

Acknowledgements

I would like to express my great gratitude to Professor Ulrich Platt for enabling me to write my bachelor thesis in his group. Many fruitful (and funny) discussions during group meetings and his vast knowledge and experience, have shed light on many new topics and approaches which have shaped this thesis. I would also like to thank Professor Thomas Wagner for being my second examiner.

Many thanks are due to Nicole Bobrowski for her knowledge not only on atmospheric and plume chemistry but also on her expertise on volcanoes and especially on Mt. Etna with both of which she enabled me to gain valuable insights and provide me with helpful tips, suggestions and new ideas. I would also like to thank her for her patience and the stress she took upon her to accommodate us and show us around during the field campaign at Mt. Etna.

My thanks also go to Jonas Kuhn and Christopher Fuchs for mentoring me during this thesis and always offering a sympathetic ear. Their constant input and support, whether there were theoretical or technical difficulties, were the main things to drive this work forward. Their revisions have greatly helped me while writing this thesis.

Furthermore, I would like to warmly thank Dieter Aletter for constructing the CL O_3 monitor and providing the O_3 generator as well as other components. His experience and support, whether it came in form of informational and instructional emails or detailed and illustrated repair instructions, have greatly helped to resolve technical issues.

Last but not least, I would like to thank Moritz Sturm for being my pillar of support when writing this thesis as well as his proofreading and revisions. Many thanks also go to Nina Lüthi, my sister and my parents for their proofreading and suggestions.

References

Bedienungshandbuch - Ozon Analysator Modell 8002, uPK Umwelt- und Prozess-Kontroll-GmbH, Bendix.

Operation manual Model POM, URL https://www.google.com/url?sa=t&rct=j&q=&esrc=s&source=web&cd=&ved=2ahUKEwj-ytKClv3sAhWInaQKHQceDSAQFjAAegQIBRAC&url=https%3A%2F%2Ftwobtech.com%2Fdocs%2Fmanuals%2Fmodel_POM_revC.pdf&usg=AOvVaw139xnrxUS9hme7gd2yQL2u, 2B Technologies, 2020.

Aletter, D.: Bedienungsanleitung in Kurzform; Immissions Ozonmonitor für Messungen in Vulkan Rauchfahnen (Prototyp 1), mLW Messtechnik für Luft und Wasserreinhaltung, 2020.

Atkinson, R., Baulch, D. L., Cox, R. A., Hampson, R. F., Kerr, J. A., Rossi, M. J., and Troe, J.: Evaluated Kinetic and Photochemical Data for Atmospheric Chemistry: Supplement VIII, Halogen Species Evaluation for Atmospheric Chemistry, Journal of Physical and Chemical Reference Data, 29, 167–266, https://doi.org/10.1063/1.556058, URL https://doi.org/10.1063/1.556058, 2000.

Atkinson, R., Baulch, D. L., Cox, R. A., Crowley, J. N., Hampson, R. F., Hynes, R. G., Jenkin, M. E., Rossi, M. J., Troe, J., and Subcommittee, I.: Evaluated kinetic and photochemical data for atmospheric chemistry: Volume II, gas phase reactions of organic species, Atmospheric Chemistry and Physics, 6, 3625–4055, https://doi.org/10.5194/acp-6-3625-2006, URL https://acp.copernicus.org/articles/6/3625/2006/, 2006.

Baicker, J. A.: Durk Current in Photomultipliers, IRE TRANSACTIONS ON NUCLEAR SCIENCE.

Barnes, I. and McGrath, W.: The chemiluminescent reaction of ozone with ketene, Journal of Photochemistry, 33, 137 – 143, https://doi.org/https://doi.org/10.1016/0047-2670(86)87028-9, URL http://www.sciencedirect.com/science/article/pii/0047267086870289, 1986.

Barrie, L. and Platt, U.: Arctic tropospheric chemistry: an overview, Tellus B: Chemical and Physical Meteorology, 49, 450–454, https://doi.org/10.3402/tellusb.v49i5.15984, URL https://doi.org/10.3402/tellusb.v49i5.15984, 1997.

Bechmann, W. and Bald, I.: Einstieg in die Physikalische Chemie für Naturwissenschaftler, Springer Spektrum (Springer-Verlag GmbH, Springer Nature), Berlin, Heidelberg,Heidelberger Platz 3, 14197 Berlin, Germany, 2017.

Bobrowski, N. and Platt, U.: SO2/BrO ratios studied in five volcanic plumes, Journal of Volcanology and Geothermal Research, 166, 147 – 160, https://doi.org/https://doi.org/10.1016/j.jvolgeores.2007.07.003, URL http://www.sciencedirect.com/science/article/pii/S037702730700220X, 2007.

Bobrowski, N., Hönninger, G., Galle, B., and Platt, U.: Detection of bromine monoxide in a volcanic plume, Nature, 423, 273 – 276, https://doi.org/https://doi.org/10.1038/nature01625, 2003.

Bobrowski, N., von Glasow, R., Aiuppa, A., Inguaggiato, S., Louban, I., Ibrahim, O. W., and Platt, U.: Reactive halogen chemistry in volcanic plumes, Journal of Geophysical Research: Atmospheres, 112, https://doi.org/https://doi.org/10.1029/2006JD007206, URL https://agupubs.onlinelibrary.wiley.com/doi/abs/10.1029/2006JD007206, 2007.

Boichu, M., Oppenheimer, C., Roberts, T. J., Tsanev, V., and Kyle, P. R.: On bromine, nitrogen oxides and ozone depletion in the tropospheric plume of Erebus volcano (Antarctica), Atmospheric Environment, 45, 3856–3866, https://doi.org/https://doi.org/10.1016/j.atmosenv.2011.03.027, URL https://www.sciencedirect.com/science/article/pii/S1352231011002640, 2011.

Branca, S. and Del Carlo, P.: Eruptions of Mt. Etna During the Past 3,200 Years: a Revised Compilation Integrating the Historical and Stratigraphic Records, pp. 1–27, American Geophysical Union (AGU), https://doi.org/https://doi.org/10.1029/143GM02, URL https://agupubs.onlinelibrary.wiley.com/doi/abs/10.1029/143GM02, 2004.

Branca, S., Coltelli, M., and Groppelli, G.: Geological Evolution of Etna Volcano, pp. 49–63, American Geophysical Union (AGU), https://doi.org/https://doi.org/10.1029/143GM04, URL https://agupubs.onlinelibrary.wiley.com/doi/abs/10.1029/143GM04, 2004.

Burton, M., Allard, P., Muré, F., and La Spina, A.: Magmatic gas composition reveals the source depth of slug-driven strombolian explosive activity., Science, 227-230, 131 – 142, https://doi.org/10.1126/science.1141900, 2007.

Carn, S. A., Froyd, K. D., Anderson, B. E., Wennberg, P., Crounse, J., Spencer, K., Dibb, J. E., Krotkov, N. A., Browell, E. V., Hair, J. W., Diskin, G., Sachse, G., and Vay, S. A.: In situ measurements of tropospheric volcanic plumes in Ecuador and Colombia during TC4, Journal of Geophysical Research: Atmospheres, 116, https://doi.org/https://doi.org/10.1029/2010JD014718, URL https://agupubs.onlinelibrary.wiley.com/doi/abs/10.1029/2010JD014718, 2011.

Donaldson, D. and Wren, S.: CHEMISTRY OF THE ATMOSPHERE | Laboratory Kinetics, in: Encyclopedia of Atmospheric Sciences (Second Edition), edited by North, G. R., Pyle, J., and Zhang, F., pp. 356 – 362, Academic Press, Oxford, second edition edn., https://doi.org/https://doi.org/10.1016/B978-0-12-382225-3.00475-8, URL http://www.sciencedirect.com/science/article/pii/B9780123822253004758, 2015.

Einstein, A.: Über die von der molekularkinetischen Theorie der Wärme geforderte Bewegung von in ruhenden Flüssigkeiten suspendierten Teilchen, Annalen der Physik, 322, 549–560, https://doi.org/https://doi.org/10.1002/andp.19053220806, URL https://onlinelibrary.wiley.com/doi/abs/10.1002/andp.19053220806, 1905.

Finlayson, B. J., Pitts, J. N., and Atkinson, R.: Low-pressure gas-phase ozone-olefin reactions. Chemiluminescence, kinetics, and mechanisms, Journal of the American Chemical Society, 96, 5356–5367, https://doi.org/10.1021/ja00824a009, URL https://doi.org/10.1021/ja00824a009, 1974.

Fruchter, J. S., Robertson, D. E., Evans, J. C., Olsen, K. B., Lepel, E. A., Laul, J. C., Abel, K. H., Sanders, R. W., Jackson, P. O., Wogman, N. S., Perkins, R. W., VAN Tuyl, H. H., Beauchamp, R. H., Shade, J. W., Daniel, J. L., Erikson, R. L., Sehmel, G. A., Lee, R. N., Robinson, A. V., Moss, O. R., and Cannon, W. C.: Mount st. Helens ash from the 18 may 1980 eruption: chemical, physical, mineralogical, and biological properties, Science (New York, N.Y.), 209(4461), 1116–1125, https://doi.org/https://doi.org/10.1126/science.209.4461.1116, 1980.

Gerlach, T. M.: Volcanic sources of tropospheric ozone-depleting trace gases, Geochemistry, Geophysics, Geosystems, 5, https://doi.org/https://doi.org/10.1029/2004GC000747, URL https://agupubs.onlinelibrary.wiley.com/doi/abs/10.1029/2004GC000747, 2004.

Herr, S.: Entwicklung eines LED basierten Ozonmonitors, Bachelorarbeit, 2011.

Hobbs, P. V., Tuell, J. P., Hegg, D. A., Radke, L. F., and Eltgroth, M. W.: Particles and gases in the emissions from the 1980–1981 volcanic eruptions of Mt. St. Helens, Journal of Geophysical Research: Oceans, 87, 11 062–11 086, https://doi.org/https://doi.org/10.1029/JC087iC13p11062, URL https://agupubs.onlinelibrary.wiley.com/doi/abs/10.1029/JC087iC13p11062, 1982.

Jourdain, L., Roberts, T. J., Pirre, M., and Josse, B.: Modeling the reactive halogen plume from Ambrym and its impact on the troposphere with the CCATT-BRAMS mesoscale model, Atmospheric Chemistry and Physics, 16, 12 099–12 125, https://doi.org/10.5194/acp-16-12099-2016, URL https://acp.copernicus.org/articles/16/12099/2016/, 2016.

Kelly, P. J., Kern, C., Roberts, T. J., Lopez, T., Werner, C., and Aiuppa, A.: Rapid chemical evolution of tropospheric volcanic emissions from Redoubt Volcano, Alaska, based on observations of ozone and halogen-containing gases, Journal of Volcanology and Geothermal Research, 259, 317 – 333, https://doi.org/https://doi.org/10.1016/j.jvolgeores.2012.04.023, URL http://www.sciencedirect.com/science/article/pii/S0377027312001230, the 2009 Eruption of Redoubt Volcano, Alaska, 2013.

Kern, C., Sihler, H., Vogel, L., Rivera, C., Herrera, M., and Platt, U.: Halogen oxide measurements at Masaya Volcano, Nicaragua using active long path differential optical absorption spectroscopy, Bulletin of Volcanology, 71, 659–670, https://doi.org/10.1007/s00445-008-0252-8, 2009.

Kleindienst, T. E., Hudgens, E. E., Smith, D. F., McElroy, F. F., and Bufalini, J. J.: Comparison of Chemiluminescence and Ultraviolet Ozone Monitor Responses in the Presence of Humidity and Photochemical Pollutants, Air & Waste, 43, 213–222, https://doi.org/10.1080/1073161X.1993.10467128, URL https://doi.org/10.1080/1073161X.1993.10467128, 1993.

Lee, C., Kim, Y. J., Tanimoto, H., Bobrowski, N., Platt, U., Mori, T., Yamamoto, K., and Hong, C. S.: High ClO and ozone depletion observed in the plume of Sakurajima volcano, Japan, Geophysical Research Letters, 32, https://doi.org/https://doi.org/10.1029/2005GL023785, URL https://agupubs.onlinelibrary.wiley.com/doi/abs/10.1029/2005GL023785, 2005.

Leston, A. R., Ollison, W. M., Spicer, C. W., and Satola, J.: Potential Interference Bias in Ozone Standard Compliance Monitoring, Journal of the Air & Waste Management Association, 55, 1464–1472, https://doi.org/10.1080/10473289.2005.10464749, URL https://doi.org/10.1080/10473289.2005.10464749, pMID: 28086057, 2005.

Olzmann, M., Kraka, E., Cremer, D., Gutbrod, R., and Andersson, S.: Energetics, Kinetics, and Product Distributions of the Reactions of Ozone with Ethene and 2,3-Dimethyl-2-butene, The Journal of Physical Chemistry A, 101, 9421–9429, https://doi.org/10.1021/jp971663e, URL https://doi.org/10.1021/jp971663e, 1997.

O'Neal, H. E. and Blumstein, C.: A new mechanism for gas phase ozone–olefin reactions, International Journal of Chemical Kinetics, 5, 397–413, https://doi.org/https://doi.org/10.1002/kin.550050310, URL https://onlinelibrary.wiley.com/doi/abs/10.1002/kin.550050310, 1973.

Platt, U. and Bobrowski, N.: Quantification of volcanic reactive halogen emissions, p. 115–132, Cambridge University Press, https://doi.org/10.1017/CBO9781107415683.011, 2015.

Radke, L. F., Hobbs, P. V., and Stith, J. L.: Airborne measurements of gases and aerosols from volcanic vents on Mt. Baker, Geophysical Research Letters, 3, 93–96, https://doi.org/https://doi.org/10.1029/GL003i002p00093, URL https://agupubs.onlinelibrary.wiley.com/doi/abs/10.1029/GL003i002p00093, 1976.

Roberts, T. J.: Ozone Depletion in Tropospheric Volcanic Plumes: From Halogen-Poor to Halogen-Rich Emissions, Geosciences, 8, https://doi.org/10.3390/geosciences8020068, URL https://www.mdpi.com/2076-3263/8/2/68, 2018.

Robock, A.: Volcanic eruptions and climate, Reviews of Geophysics, 38, 191–219, https://doi.org/https://doi.org/10.1029/1998RG000054, URL https://agupubs.onlinelibrary.wiley.com/doi/abs/10.1029/1998RG000054, 2000.

Roedel, W. and Wagner, T.: Physik unserer Umwelt: Die Atmosphäre, Springer Spektrum, Berlin, Heidelberg, 2017.

Rüdiger, J., Tirpitz, J.-L., de Moor, J. M., Bobrowski, N., Gutmann, A., Liuzzo, M., Ibarra, M., and Hoffmann, T.: Implementation of electrochemical, optical and denuder-based sensors and sampling techniques on UAV for volcanic gas measurements: examples from Masaya, Turrialba and Stromboli volcanoes, Atmospheric Measurement Techniques, 11, 2441–2457, https://doi.org/10.5194/amt-11-2441-2018, URL https://amt.copernicus.org/articles/11/2441/2018/, 2018.

Rüdiger, J., Schmitt, S., Wittmer, J., Bednorz, A., and Einhorn, A.: Final report for Research Project „Reaktive Halogene in einer simulierten Vulkanfahne“, 2020.

Surl, L., Donohoue, D., Aiuppa, A., Bobrowski, N., and von Glasow, R.: Quantification of the depletion of ozone in the plume of Mount Etna, Atmospheric Chemistry and Physics, 15, 2613–2628, https://doi.org/10.5194/acp-15-2613-2015, URL https://acp.copernicus.org/articles/15/2613/2015/, 2015.

Vance, A., McGonigle, A. J. S., Aiuppa, A., Stith, J. L., Turnbull, K., and von Glasow, R.: Ozone depletion in tropospheric volcanic plumes, Geophysical Research Letters, 37, https://doi.org/https://doi.org/10.1029/2010GL044997, URL https://agupubs.onlinelibrary.wiley.com/doi/abs/10.1029/2010GL044997, 2010.

von Glasow, R.: Atmospheric chemistry in volcanic plumes, Proceedings of the National Academy of Sciences, 107, 6594–6599, https://doi.org/10.1073/pnas.0913164107, URL https://www.pnas.org/content/107/15/6594, 2010.

von Glasow, R., Bobrowski, N., and Kern, C.: The effects of volcanic eruptions on atmospheric chemistry, Chemical Geology, 263, 131 – 142, https://doi.org/https://doi.org/10.1016/j.chemgeo.2008.08.020, URL http://www.sciencedirect.com/science/article/pii/S0009254108003756, halogens in Volcanic Systems and Their Environmental Impacts, 2009.

Wennberg, P.: Atmospheric chemistry: Bromine explosion, Nature, 397, 299–301, 1999.

Williams, E. J., Fehsenfeld, F. C., Jobson, B. T., Kuster, W. C., Goldan, P. D., Stutz, J., and McClenny, W. A.: Comparison of Ultraviolet Absorbance, Chemiluminescence, and DOAS Instruments for Ambient Ozone Monitoring, Environmental Science & Technology, 40, 5755–5762, https://doi.org/10.1021/es0523542, URL https://doi.org/10.1021/es0523542, pMID: 17007137, 2006.

Zahn, A., Weppner, J., Widmann, H., Schlote-Holubek, K., Burger, B., Kühner, T., and Franke, H.: A fast and precise chemiluminescence ozone detector for eddy flux and airborne application, Atmospheric Measurement Techniques, 5, 363–375, https://doi.org/10.5194/amt-5-363-2012, URL https://amt.copernicus.org/articles/5/363/2012/, 2012.

Appendices

Wiring diagrams of Arduino

The wiring diagrams shown in the following are adapted form the wiring diagrams of Dieter Aletter, which are shown in the manual Aletter (2020). The diagrams shown here include smaller changes which were performed during the course of this thesis.

Verdrahtung Arduino Module: ÜBERBLICK

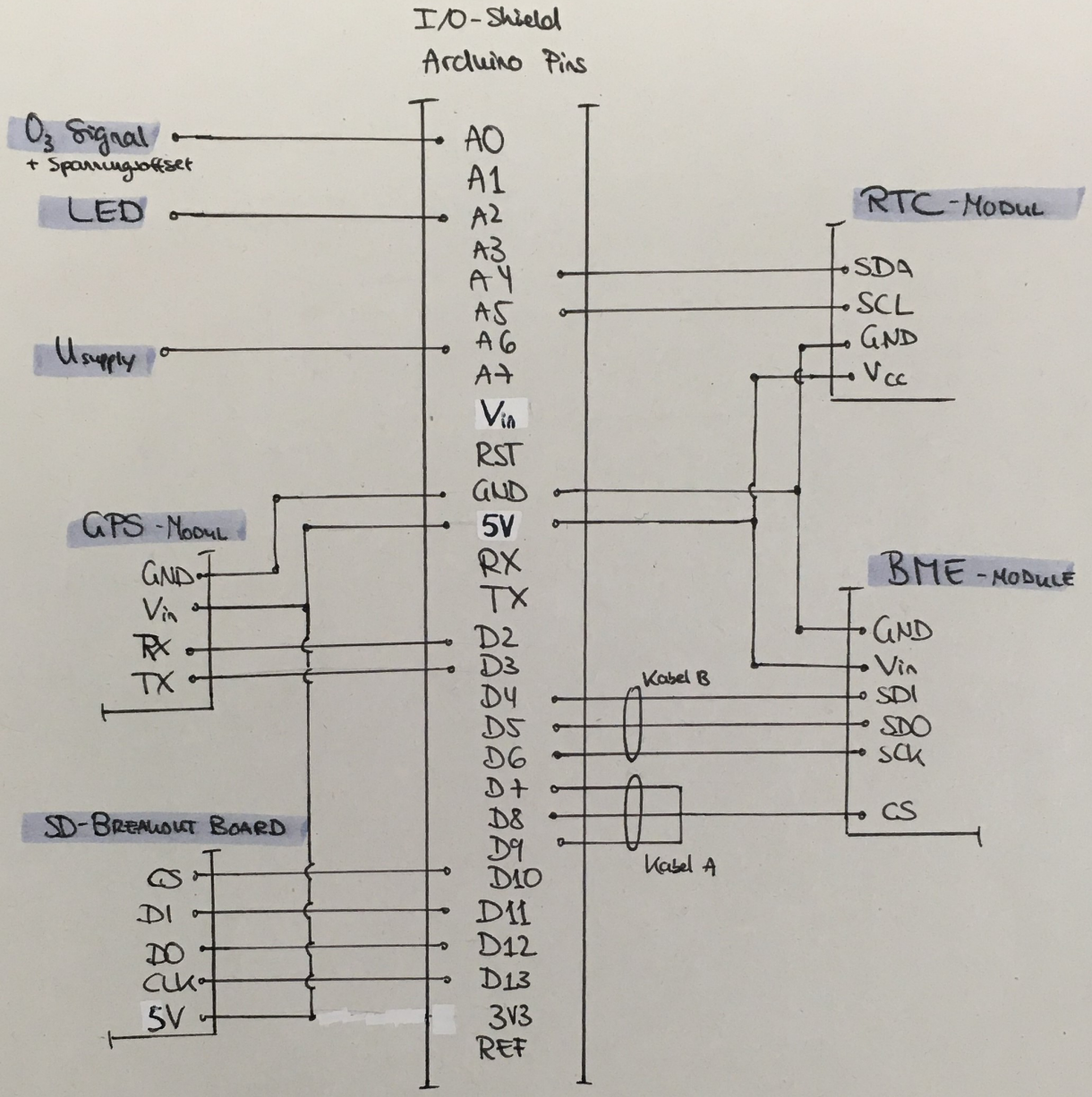

Verdrahtung Arduino Module: O3 Signal, Usupply, LED

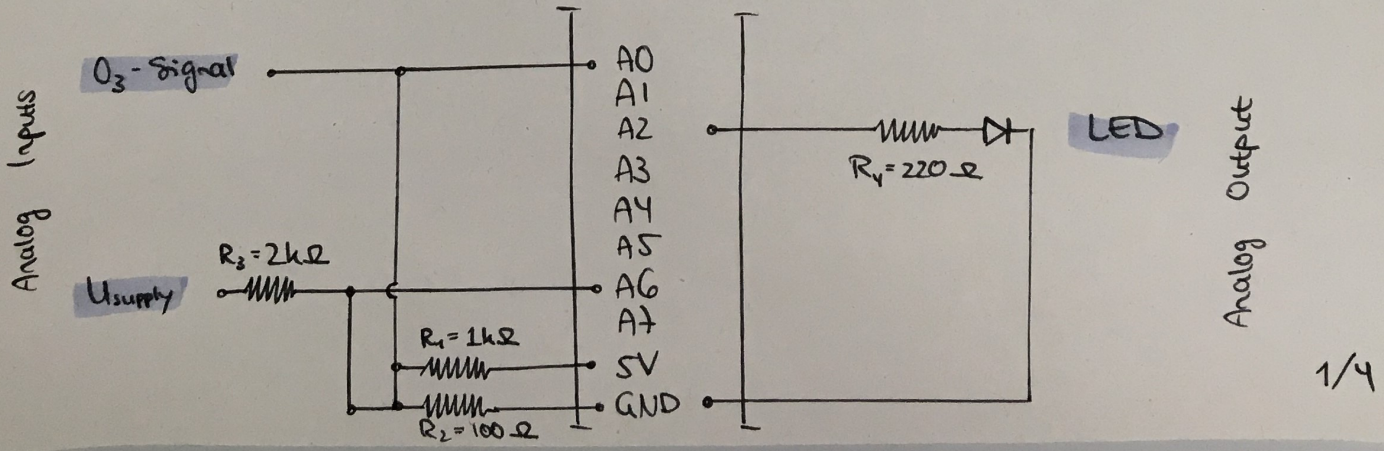

1/4

Verdrahtung Arduino Module : GPS-, SD-, RTC-Modul

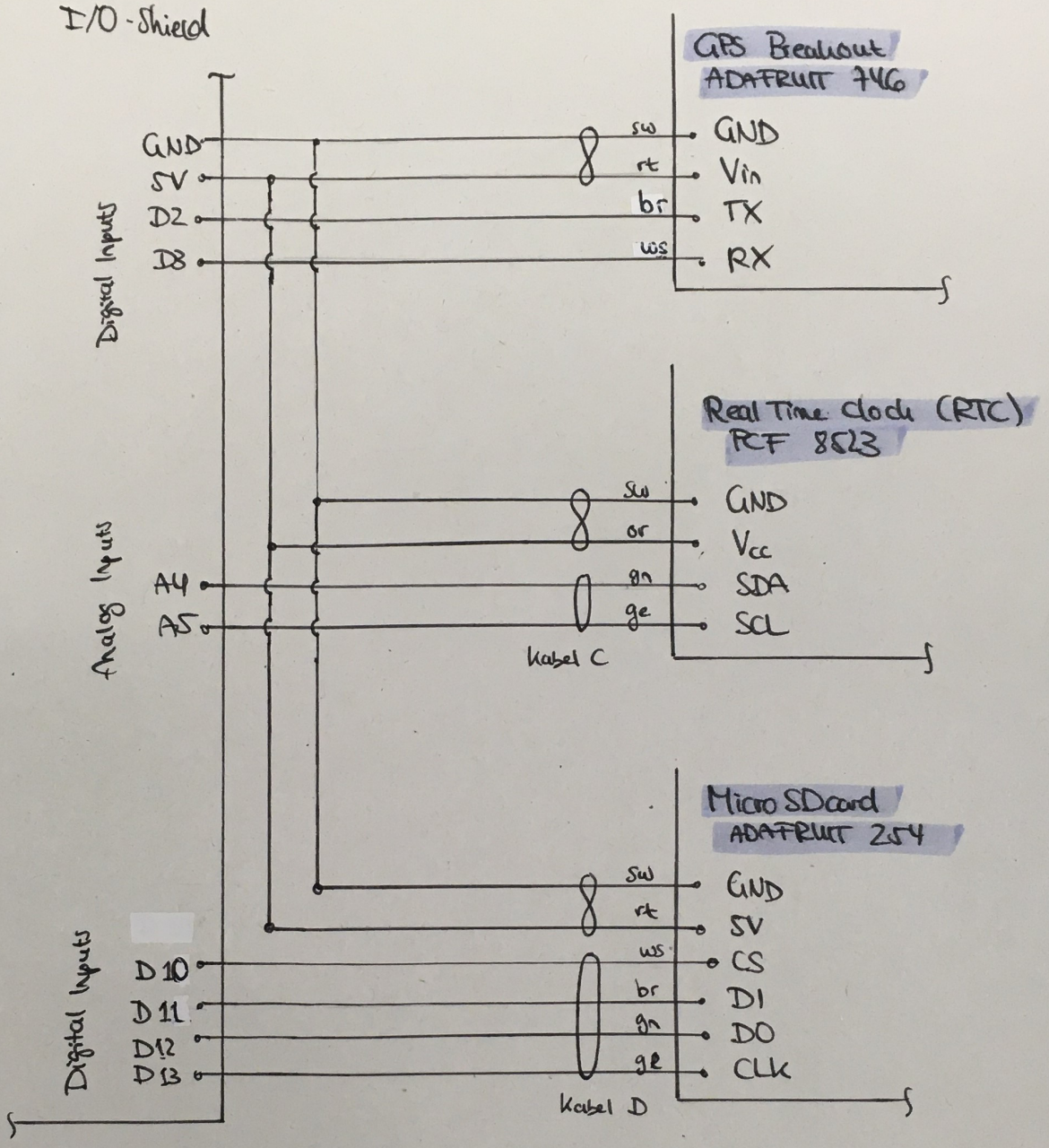

∞ ≙ verdrillt

sw ≙ schwarz
rt ≙ rot
Or ≙ orange
ge ≙ gelb
gn ≙ grün
br ≙ braun
ws ≙ weiß

2/4

Verdrahtung Arduino Module : BME TEMPERATURSENSOREN

THP-MODULE, ADAFRUIT BME 280

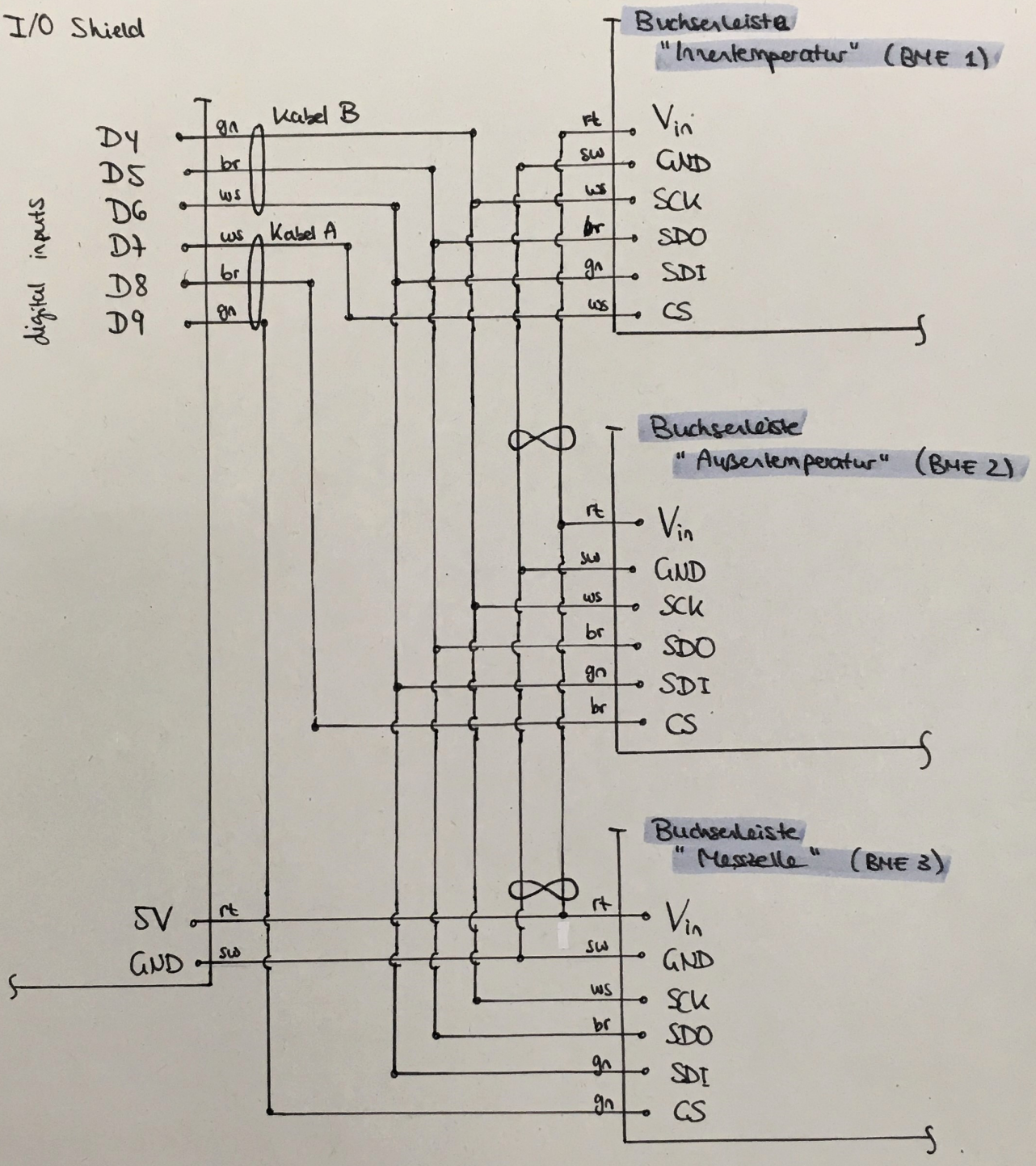

3/4

Verdrahtung Arduino Module:

STIFLEISTE BME-MODULE
THP-MODULE, ADAFRUIT BME 280

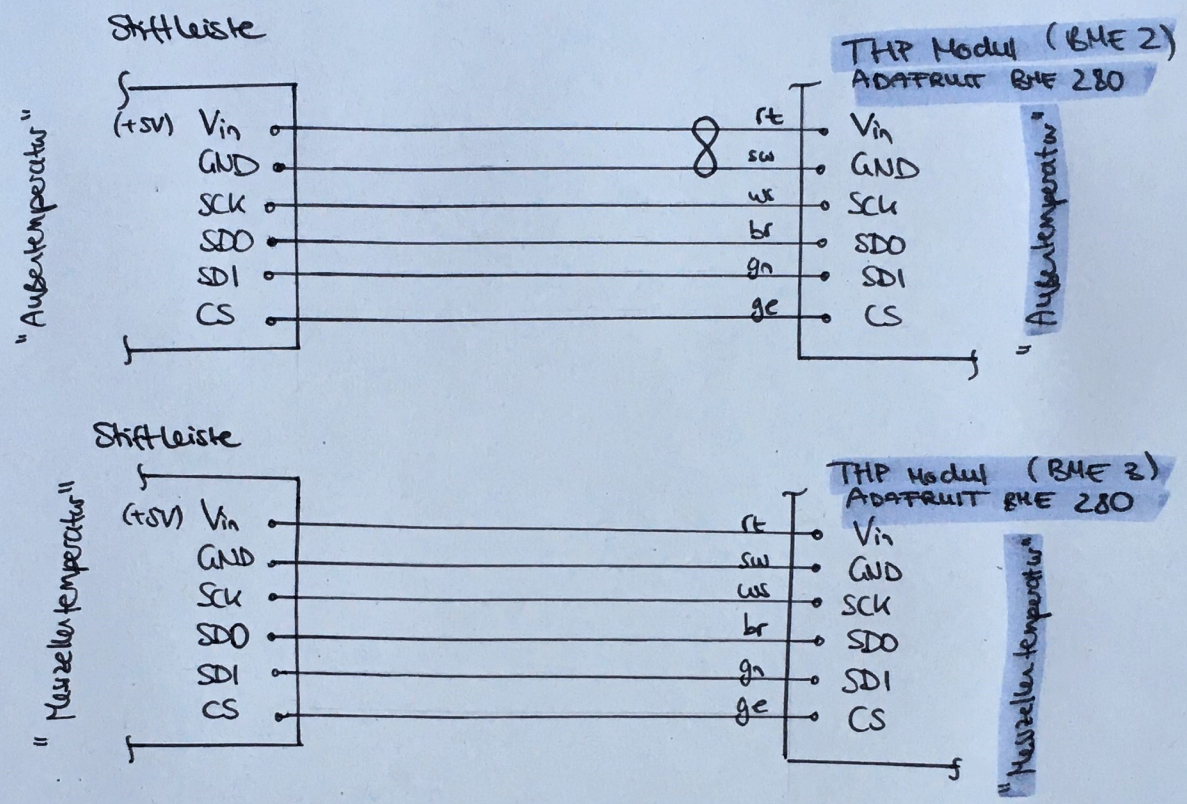

4/4

Erklärung

Ich versichere, dass ich diese Arbeit selbstständig verfasst und keine anderen als die angegebenen Quellen und Hilfsmittel benutzt habe.

Heidelberg, den 07.03.2021,

M. Rüth